2022

Wireless Power Transfer In Autonomous Mobile Microgrids

Carl Greene
Michigan Technological University, carlg@mtu.edu

WIRELESS POWER TRANSFER IN AUTONOMOUS MOBILE MICROGRIDS

By

Carl S. Greene

A THESIS

Submitted in partial fulfillment of the requirements for the degree of

MASTER OF SCIENCE

In Mechanical Engineering

MICHIGAN TECHNOLOGICAL UNIVERSITY

2022

This thesis has been approved in partial fulfillment of the requirements for the Degree of MASTER OF SCIENCE in Mechanical Engineering.

Department of Mechanical Engineering - Engineering Mechanics

Thesis Advisor: *Dr. Wayne W. Weaver*

Committee Member: *Dr. Jeremy P. Bos*

Committee Member: *Dr. Gordon G. Parker*

Department Chair: *Dr. William W. Predebon*

Dedication

To my mother and father, who instilled in me the value of education and fostered my love of science.

Contents

List of Figures

Preface

The following work presented in this thesis is part of the research conducted from 2018-2021 through the Center for Agile and Interconnected Micro-grids (AIM) at Michigan Technological University. Incorporating wireless power transfer into autonomous mobile micro-grids was one of the main objectives of this work.

Chapter 1.4 is an introduction to this area of study and summarizing the current technologies, obstacles to over come, and applications of said technologies. In **Chapter 2** the background of previous work in wireless power transfer, autonomous mobile micro-grids and unmanned ground vehicle (UGV) docking is discussed. **Chapter 3** is an in-depth look at the hardware and software used in the project. Differing methods of data analysis as well as protocols are also explored. **Chapter 4** is a summary of the results of the experimentation done with the orientation of the hardware and software discussed in **Chapter 3**. **Chapter 5** summarizes the findings and concludes this work; considerations of future work are also discussed.

Acknowledgments

I would like to thank the members of our research lab who contributed to work and publications found in this research, including Dr. Wayne Weaver, Dr. Jeremy Bos, Dr. John Naglak, Casey Majhor, Caleb Kase, and Max McGinty.

Special thanks to Dr. Wayne Weaver, for his patience and guidance throughout the course of my studies.

I wish to thank my committee members Dr. Jeremy Bos and Dr. Gordon Parker for their insight and support.

Additionally, I would like to thank the U.S. Office of Naval Research for their support on this research project. This work was supported by the U.S. Office of Naval Research under Award N00014-16-1-2422 and does not reflect their views or opinions.

Lastly, I would like to thank my partner, Breanna, for her tremendous support throughout my academic career.

List of Abbreviations

WPT	Wireless Power Transfer
PV	Photovoltaic
UGV	Unmanned Ground Vehicle
AUV	Autonomous Underwater Vehicle
COTS	Commercial-Off-the-Shelf
DOF	Degree of Freedom
FOV	Field of View
EMI	Electromagnetic Interference
DoD	Department of Defense
GPS	Global Positioning System
IMU	Inerital Measurement Unit
LiDAR	Light Detection And Ranging
ROS	Robot Operating System
USB	Universal Serial Bus
GPU	Graphics Processing Unit
IC	Integrated Circuit
I2C	Inter-Integrated Circuit
RTC	Real-Time Clock

SCL	Serial Clock Line
SDA	Serial Data Line
SOC	State of Charge
AIM	Agile and Interconnected Microgrids
ART	Augmented Reality Tag
CPU	Central Processing Unit
DGR	Distributed Generation Resource
FOB	Forward Operating Base
GA	Genetic Algorithm
ISR	Intelligence, Surveillance, and Reconnaissance
JSP	Job-Shop Scheduling Problem
NP	Non-deterministic Polynomial-time
SMS	Single Machine Scheduling
UAV	Unmanned Aerial Vehicle
VSDS	Variable-Size Design Space
WSN	Wireless Sensor Network

Abstract

The ability to autonomously dock unmanned ground vehicles plays a key role in mobile micro-grids, where efficient power transfer is paramount. The approach utilized in this work allows for near-field wireless power transfer in remote locations with minimal support. Establishing a micro-grid power system connection autonomously using wireless power eliminates the arduous task of designing a complex, multiple degrees of freedom (MDOF) robotic arm. The work presented in this thesis focuses on both the hardware and software within the micro-grid system. This particular near-field wireless system consists of a primary and secondary set of modules, comprised of Litz wire coils, which are inductively coupled to complete the circuit. Both the primary and secondary modules contain a shunt resistor circuit, as well as a potential divider circuit and an Arduino controller (used to collect and analyze recorded data). The aforementioned hardware, allows for quantitative measurements of voltage, current, and power of the primary and secondary modules. Robot rover docking is accomplished using camera visualization, wheel odometry, and GPS data, all of which, are provided by the Robot Operating System (ROS). Various docking poses are used to characterize overall power transfer and efficiency at diverse alignments. Using collected data from the near field power modules' Arduino controllers and ROS, power from the coils is measured as functions of both the distance between coils and associated yaw angle. Power transfer efficiency is then evaluated using compiled power

data. A dynamic feedback control system optimizes power transfer efficiency and docking alignment. The camera visual feedback control system acts as the driving force for re-docking the robot, further enhancing efficiency of the proposed near field power connection. In its entirety, this research explores the physical and mathematical relationships used to develop a dynamic feedback control system.

Chapter 1

Introduction

To many, electrical power is something taken for granted daily. It is a commodity that people may not take the time to appreciate or understand the vast systems that provide them with this critical resource. If one were to speak of the "power grid" many will only be able to relate to the topical headlines that they hear on the news regarding the failures of such systems. The micro-grid is a relatively new technological concept that is being implemented worldwide to solve much power and sometimes other unique issues. Micro-grids are modular systems and can provide controllable energy resources in many different forms. There are many examples of micro-grids equipped with fuel cells, photovoltaics (PV), combustion generators, wind generators, and battery storage. With the various energy resources, the micro-grid can provide localized renewable clean energy that can be robust and efficient.

In the following, we will explore a subset of a micro-grid system, specifically, the deployment of an autonomous mobile micro-grid and several features incorporated to alleviate complexity within its operational range. Firstly, what is a micro-grid?

1.1 History of Micro-grid Technology

The United States power grid infrastructure first took hold with what was, at the time, an example of a micro-grid. On September 4th 1882, the Edison Illuminating Company brought the Pearl Street Station (seen in Figure 1.1) online, providing Americans with the first instance of grid connected power. On September 30th 1882, the Vulcan Street Hydroelectric Plant, located in Appleton, Wisconsin (Figure 1.2), was spun-up, providing Wisconsin with grid connected power as the first hydroelectric power station in the United States.

Both instances mentioned above are examples of micro-grid systems in there infancy; when there was a limited amount of power generation, loads, and storage capacity. Initially, these were isolated systems without any interconnections to other power or central stations. As industrial and consumer electrical power demand grew, the isolated power stations were not enough to meet demand. This is when power stations first began to be connected into a network or grid. At the time there were

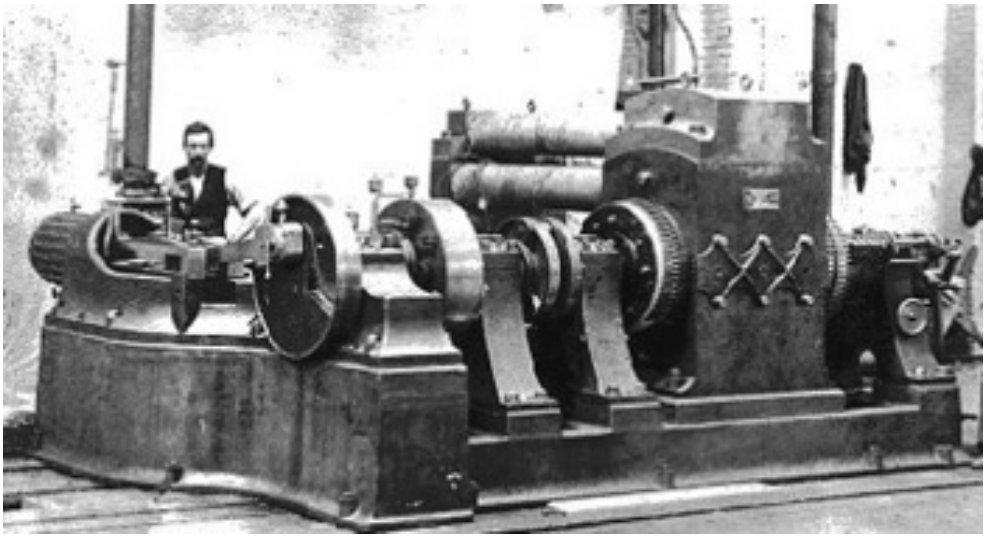

Figure 1.1: Pearl Street Station dynamo

[1]

many different systems providing power in different forms, direct or alternating current, as well as varying frequencies. In 1926, the Electricity Supply Act established the specifications for a National Grid, which provided the foundation of our power infrastructure.

1.2 Where are Autonomous Mobile Micro-grids?

More than 100 years later, micro-grids are still commonplace and evolving rapidly. There are nearly limitless applications to the systems being produced today. In the most basic sense, micro-grids consist of components in a defined boundary that can generate, consume or store energy. These systems can either be standalone or connected to an existing power grid[2][2]. Many micro-grid systems have been used to

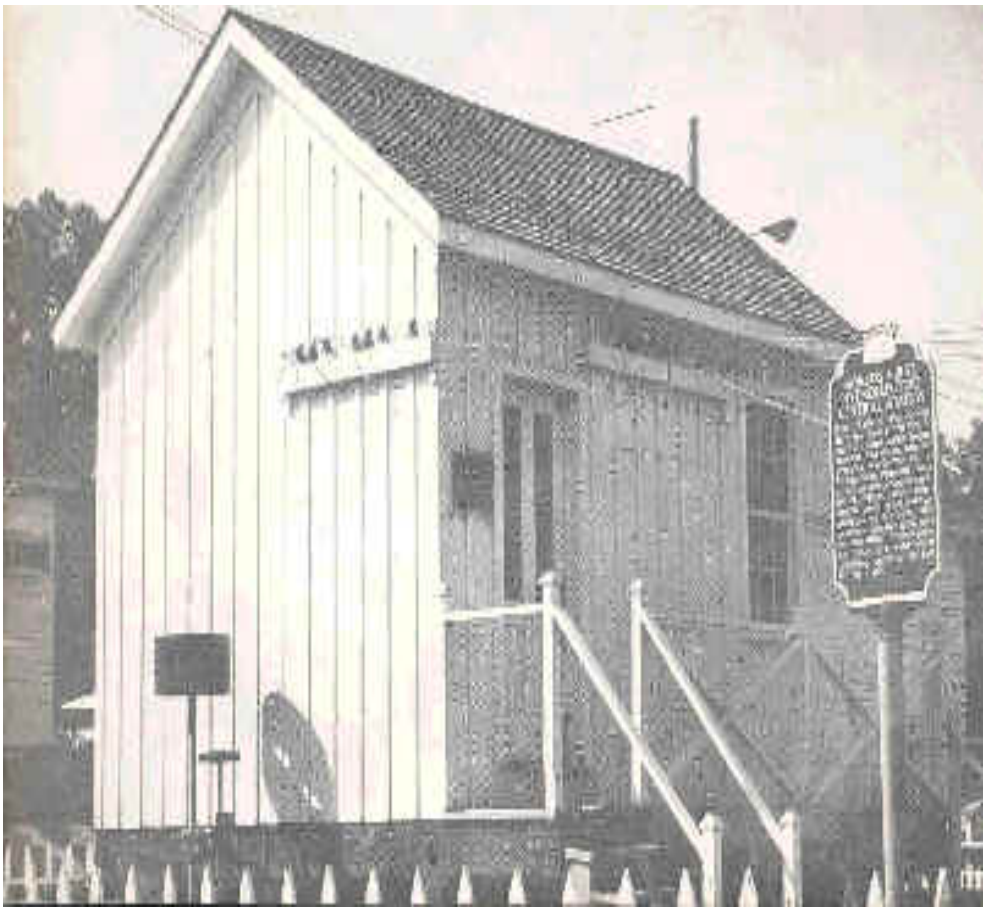

Figure 1.2: Vulcan Street Plant © IEEE. All rights reserved.

supplement the National Grid during natural disasters such as hurricanes, tornadoes, or other instances of adverse weather[3]. A unique case was the 2021 winter storm that crippled the state of Texas. This case is special because most of the state operates on the Texas Interconnection, one of only three independent power grids in the United States. Due to record cold temperatures and the isolation of the Texas Interconnection, millions of Texans' were left without power. Instances of residents utilizing their hybrid vehicles for power generation, as seen in Figures 1.3 and 1.4, appeared on the news. What many did not realize was that by doing so they had

Figure 1.3: Ford F150 connection to residential power grid.

created their very own micro-grid.

Due to the adaptability and self-sustaining nature of micro-grids, they are well suited for implementation in rural areas or in developing countries that lack the critical infrastructure of a traditional power grid. These areas can be transformed from an unrelenting challenge into more hospitable terrain with modern necessities such as light, heat, and clean water.

Recently, micro-grids have been given a boost by incorporating autonomous robots to create mobile micro-grids. This advancement has allowed for utilization in military applications and operations, which require large amounts of power and connectivity. The micro-grid is an adaptable solution to the various connectivity issues encountered

Figure 1.4: Ford F150 output power data.

in the modern era, including Forward Operating Bases (FOB) such as those described in [4], which are inherently dangerous due to their proximity to hostiles and overall purpose. Imagine a micro-grid with the ability to be heavy dropped and provide power to an FOB immediately without the arduous task of setup by soldiers (see examples of military applications of micro-grid technology in Figures 1.6 and 1.5). Such types of implementation save time and reduce risk and could very well save lives.

Furthermore, micro-grids have also been implemented in various aerospace applications for out-of-this-world employment. An example of an aerospace micro-grid

Figure 1.5: Mobile U.S. Military power generation skids.

[5]

Figure 1.6: U.S. Military solar array.

[6]

application is Project Artemis, shown in Figure 1.7, which is the next manned moon mission intending to transport the first woman and person of color to the first long-term habitation of the moon.

Figure 1.7: Artist rendering of proposed moon base.

[7]

Figure 1.8: Robotic arm on mobile micro-grid agent.

Much of the current autonomous mobile micro-grid work involves cable deployment between mobile agents, using robotic arms to connect said agents (Figure 1.8) [8][9][3]. Issues that arise from navigation precision, cable deployment, and multiple degree of freedom robotics can all be reduced by utilization of wireless power transmission [10] [11].

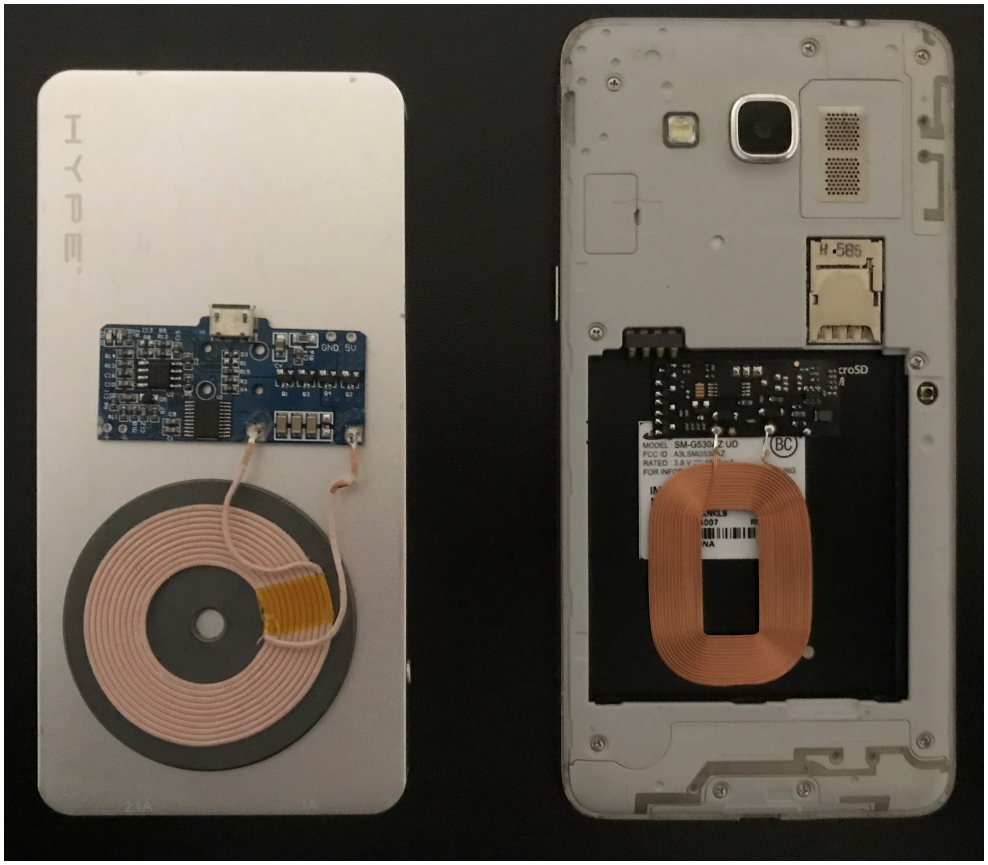

Figure 1.9: Wireless cellular phone charging hardware.

While many examples of wireless power transmitting devices are widespread on the consumer market, there are limited options for the desired performance specifications. Since most near-field wireless power systems commercially available are designed for small mobile devices, such as the one seen in Figure 1.9, and the project required significantly greater power, other viable options were explored [12]. The advancement in electric vehicles and the wireless power systems used were also researched[13]. Various automotive-style wireless charging systems proved to be prohibitive both in cost and physical dimensions [14]. The complexity of what was sought to be eliminated was similar to what was found by Wang [15].

The desired power requirement has very limited players; thus, a decision was made to combine off-the-shelf hardware for this application. Modules were then created to fit power requirements of the mission for the unmanned ground vehicle (UGV) platform, while maintaining a level of simplicity and requiring minimal support.

1.3 Contributions of this Work

The research associated with this project provides a template for near-field wireless power transmitting modules that fit within a specific performance window, which has yet to be populated. The design of this system is also applicable in micro-grid power systems and load scheduling optimization. The use of various sensors and micro-controllers to incorporate a high level of control into the near-field wireless system is demonstrated within this design. The feedback control incorporated into the robotic platform provides an innovative application of current off-the-shelf hardware. This hardware, in conjunction with the feedback control software, allows one to overcome complex and cost prohibitive robotic systems.

The following will cover the mainstays of the hardware used in the near-field wireless power transmitting modules. The software utilized to aid in UGV navigation and docking will be investigated, and the implementation of the near-field wireless power system onto the UGV platform used in this micro-grid project will also be explored.

Next, a walk-through of the validation methods used to establish the benchmarks appointed to serve as the parameters for the docking and re-docking protocol will be provided. To finalize this work, there will be a discussion on the characterization of the inductively coupled modules, the overall efficiency of the power transfer, and the success rate at which docking can be achieved. This work will show that wireless power transfer can be successfully integrated into mobile micro-grids and provide quality docking through camera visualization feedback control. This research aims to determine whether quality wireless power transfer in mobile micro-grids is achievable by the use of camera visualization as feedback control.

1.4 Thesis Organization

In preparing this thesis, portions of papers developed during this research are included. The remainder of this thesis is organized as follows: Chapter 2 examines background details of the micro-grid project as well as both previous and current work in autonomous mobile micro-grids, Chapter 3 contains the details of the hardware and software used in optimizing the mobile micro-grid wireless power transfer architecture, Chapter 4 introduces the results of experimentation as well as analysis of the system, and Chapter 5 is the conclusion of this thesis and includes future work to be considered.

Chapter 2

Background

2.1 Introduction

This chapter provides background information on the autonomous mobile micro-grid research presented in this thesis. Prior and current research on autonomous mobile micro-grids is explored as well as details pertaining to the overall project goals and deliverables. The specifications of the mobile agents used in this research work are also discussed. To conclude this chapter, the wireless power transfer system outfitted to this particular autonomous mobile micro-grid is introduced f[1].

[1]The material in this chapter is reprinted in majority from [16]

2.2 Current and Relevant Work

In the previous chapter, the micro-grid was introduced and defined as systems of interconnected, controllable energy resources and loads that reside within a defined boundary. A mobile micro-grid is a subset of these systems that implement robotic agents (i.e., unmanned ground vehicles (UGV) or unmanned aerial vehicles (UAV)) outfitted with power grid hardware including but not limited to; fuel cells, photovoltaics (PV), combustion generators, wind generators, or battery storage, an example of which is shown in Figure 2.1. With advancements in computation capability over the last decade, UGV and UAV autonomy has greatly increased. Autonomous mobile micro-grids can be remotely deployed for use in military operations, space operations, and disaster recovery, all with the flip of a switch [17][2].

An autonomous mobile micro-grid is advantageous in that it can adapt to environmental and load demand changes, thus providing system optimization. These robotic agents are linked via wireless connection in order to communicate location and mission intentions. The adaptability of these systems allows for micro-grid deployment into additional situations, such as UAV and UGV surveillance, UAV and UGV support of Wireless Sensor Networks (WSN), and under water data collection via Autonomous Underwater Vehicles (AUV) [18]. A multi-agent collaboration can be seen in Figure 2.2. An example of an autonomous mobile micro-grid deployment is explored by

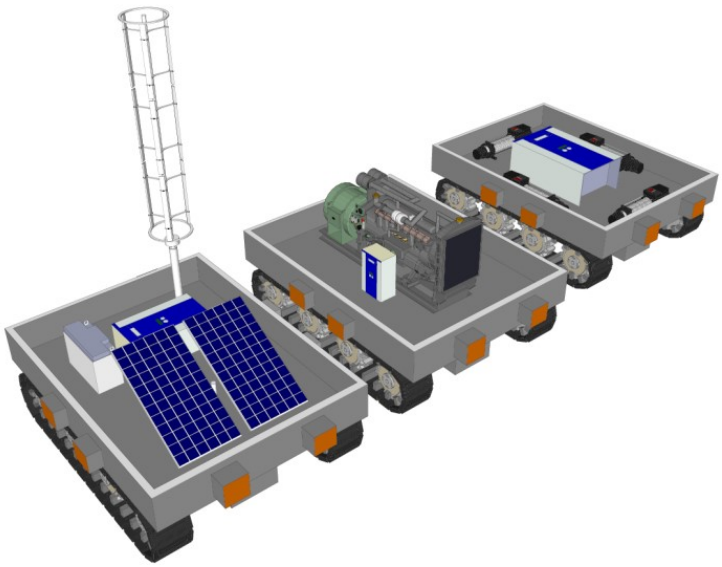

Figure 2.1: Concept image of autonomous robot energy resources with renewable sources, diesel generator and power conversion. © IEEE. All rights reserved.

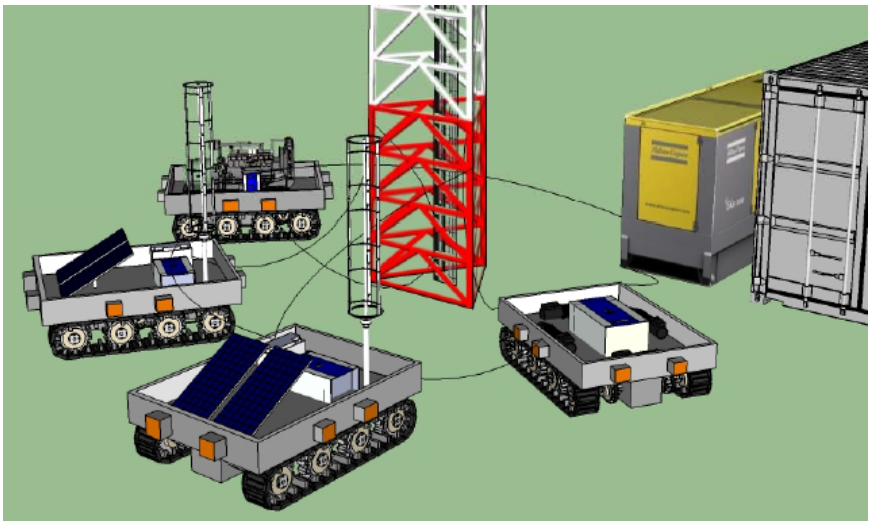

Figure 2.2: Autonomous robot energy resources positioned to power a critical load. © IEEE. All rights reserved.

Darani et al. [19], in which, a temporary micro-grid is used to power loads under various constraints . This work also exhibits the use of a genetic algorithm (GA), which

can determine the optimal positions and paths of agents and sources, therefore, providing more efficient deployments. Another example of path optimization and wireless power transfer can be found in Naglak and Majhor et al. [20][21]. These two works are directly tied to the research in this thesis. UAVs are also becoming prevalent in autonomous mobile networks, in the work by Johnson et al. [22] a UAV system allows for the recharging of agents within a WSN, while reducing overall network downtime . More similar to the work discussed later in this thesis, Angelopoulos et al. [23] demonstrates various methods to traverse an area and provide wireless power support to a WSN. Another example of wireless power support is found in Li et al. [24], where a number of UAVs act as nodes within a WSN . These unique systems open the door to rapid mission support in a in a less invasive manner.

This project was born out of necessity for evolution of the micro-grid project at Michigan Technological University (MTU) and the Center for Agile and Interconnected Micro-grids (AIM). The research team set out with several objectives as part of the project supported by the U.S. Office of Naval Research under Award N00014-16-1-2. The research team was tasked with creating an autonomous mobile micro-grid capable of identifying various assets and loads, as well as, creating power transfer connections to these agents by implementing a genetic algorithm capable of optimization and mission path planning. The mobile robotic agents had to utilize autonomous functionality to support local infrastructure and the micro-grid "loads" were represented by both fixed and mobile assets. The UGV micro-grid agents were positioned

based on the requirements for their power generation sources, and some of the UGVs were dedicated to providing electrical connection between the sources and loads. As mission requirements change, or infrastructure is reallocated, these connections need to be re-configurable [20].

2.3 UGV Platform

At the research team's disposal, were four Clearpath Husky UGVs. The Husky UGVs came equipped from the manufacturer with a Mini-ITX computer containing an Intel i5 processor, running at 2.9 GHz. The operating system on the machines is Ubuntu 14.04. The UGVs were outfitted with a sensor array including the following: a LORD MicroStrain 3DM-GX3-25 nine Degree Of Freedom (DOF) Inertial Measurement Unit (IMU) and NovAtel SMART6-L Global Positioning System (GPS) receiver, and a SICK LMS-111 2D Light Detection and Ranging (LiDAR) device. The Husky UGV is controlled using the modular open source software environment known as the Robot Operating System or ROS. This software suite allows for low-level hardware control, as well as, complex modeling and simulation [25].

2.4 UGV Hardware

Numerous modifications were made to the Husky UGVs, which provided the flexibility to deploy the mobile micro-grid under diverse mission plans. The novel hardware setup of each Husky UGV was to provide support for the power grid, which included power generation, power conversion, power storage, power transmission, and switching. The Husky UGVs were also modified with hardware to aid in the autonomous mission, which includes communication, perception, and manipulators [20][21][16].

At the time of data acquisition, sensor hardware setup on each of the Husky UGV agents, for navigational purposes, consisted of the following: a LORD MicroStrain 3DM-GX3-25 nine DOF IMU, a NovAtel SMART6-L GPS antenna, a SICK LMS-111 2D LiDAR, and a Sony Playstation Eye camera as seen in 2.3. This sensor network has been used by numerous research groups and a similar setup was used by Moridian et al. (2015) [3].

Two of the Clearpath Husky UGVs were outfitted with internal combustion gas engine generators producing a 120 VAC output and capable of providing 1000 W. This addition to the UGVs would extend the operational range and provide consistent traversal performance over various terrain-types during mission deployment. Both mobile genset agents have a 120 V AC to 24 V DC and 120 V AC to 48 V DC

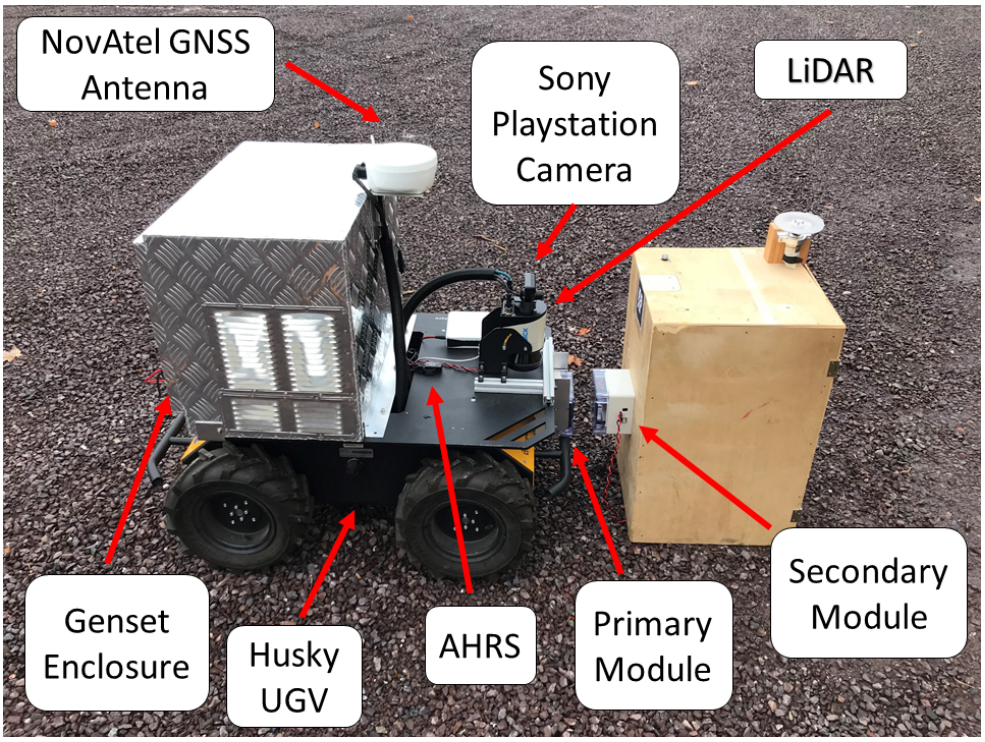

Figure 2.3: Clearpath Husky UGV provides all-terrain navigation with sufficient payload capacity for demonstration power grid hardware.

switching power supply, which was integrated into the design to provide power to the UGV chassis battery bus and load support. Due to the sensitive navigation equipment on the Husky UGVs, and the electromagnetic interference (EMI) produced by the generator and power supplies, a Faraday cage was created to house the generator and power supplies. An example of the genset Husky UGV is shown in Figure 2.4.

The design team also wanted to include a bus agent in the the autonomous mobile micro-grid. This bus agent was equipped with a 48 V DC lead acid battery module and a 48 V DC PV array. This agent was also equipped with a 48 V DC to 24 V DC switching power supply. The addition of the switching power supply allowed

Figure 2.4: Clearpath Husky UGV provides all-terrain navigation with sufficient payload capacity for demonstration power grid hardware.

for increased run time during missions by providing the Husky UGV chassis with additional 24 V DC storage capacity. The bus agent can be seen in Figure 2.5.

The remaining Husky UGV was designed to be the cabling agent (as shown in Figure 2.6). This cabling agent was to provide various connections between agents and loads, utilizing a fixed-type male and female connector that could be connected to both loads and sources. An example of the connectors can be seen in Figure 2.7 and the coupled mobile agents are shown in Figure 2.8.

Figure 2.5: Clearpath Husky UGV outfitted with 48V PV array and battery storage.

2.5 Near-Field Wireless Power Transmission

Wireless power has become commonplace in our daily lives. Though some forms of wireless power have existed for over 150 years [26], continued development and deployment of the technology seems endless [27]. With an abundant supply of commercially

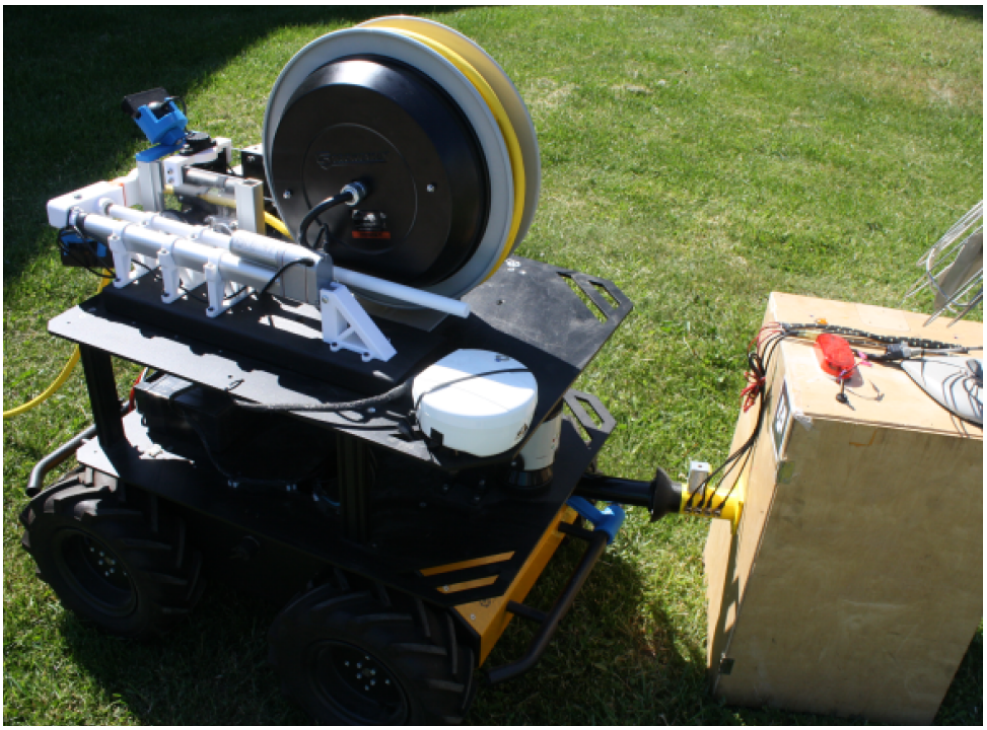

Figure 2.6: Clearpath Husky UGV provides power as a cable distribution agent.

available systems, many previously difficult tasks can be aided by near-field wireless power systems. One of our objectives for investigating the capabilities of wireless power transfer was for use in the autonomous mobile micro-grid.

Research of near-field wireless systems, currently available on the market, demonstrates numerous technologies being utilized [28]. There is a tremendous amount of work involving wireless power transfer being implemented in electric vehicle charging [29][30][31]. Each technology has their own characteristics, and thus, their own niche use. Many works investigate the different topologies and varying complex characteristics of wireless power systems[32][33][34][35][36][37]. Two widely used forms of

Figure 2.7: Clearpath Husky UGV with fixed type AC/DC power connectors.

near-field wireless power are inductive coupling and capacitive coupling. Both systems can incorporate resonance into their design to increase the distances at which the transmitting module can send power to the receiving module.

The system selected for this research project utilizes the principle of inductive coupling. Near-field wireless power transmission is achieved via inductive coupling of two separate coils of Litz wire. The Litz wire modules were chosen over other versions due to the particular characteristics of the Litz wire itself. Litz wire consists of strands of individually insulated wire that is woven together to form a group that is also insulated. This process is done in order to reduce the proximity effect which

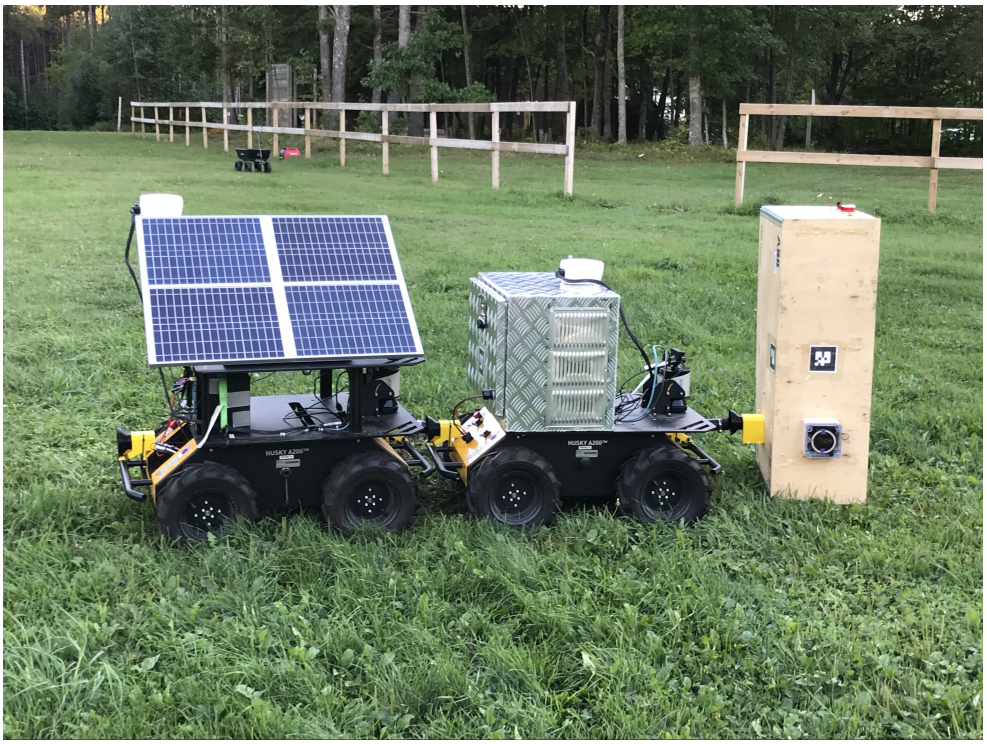

Figure 2.8: Clearpath Husky UGV agents coupled providing load support.

causes increased resistance in conductors that are in close proximity to one another with alternating current passing [38]. The system is comprised of a "primary" (or transmitting) side module that is mounted to the mobile bus agent. The "secondary" (or receiving) side module is mounted to the stationary load. The near-field wireless power transmission system works on the principle of inductive coupling, wherein, the process of inductive coupling can be thought of as sending power from one coil of wire (or primary coil) to another coil of wire (or secondary coil) without a physical connection between the aforementioned coils. The transmitting and receiving modules have no physical connection between one another. Power is transferred due to the magnetic flux from the transmitting module inducing an alternating current on the receiving module coil, as depicted in Figure 2.9.

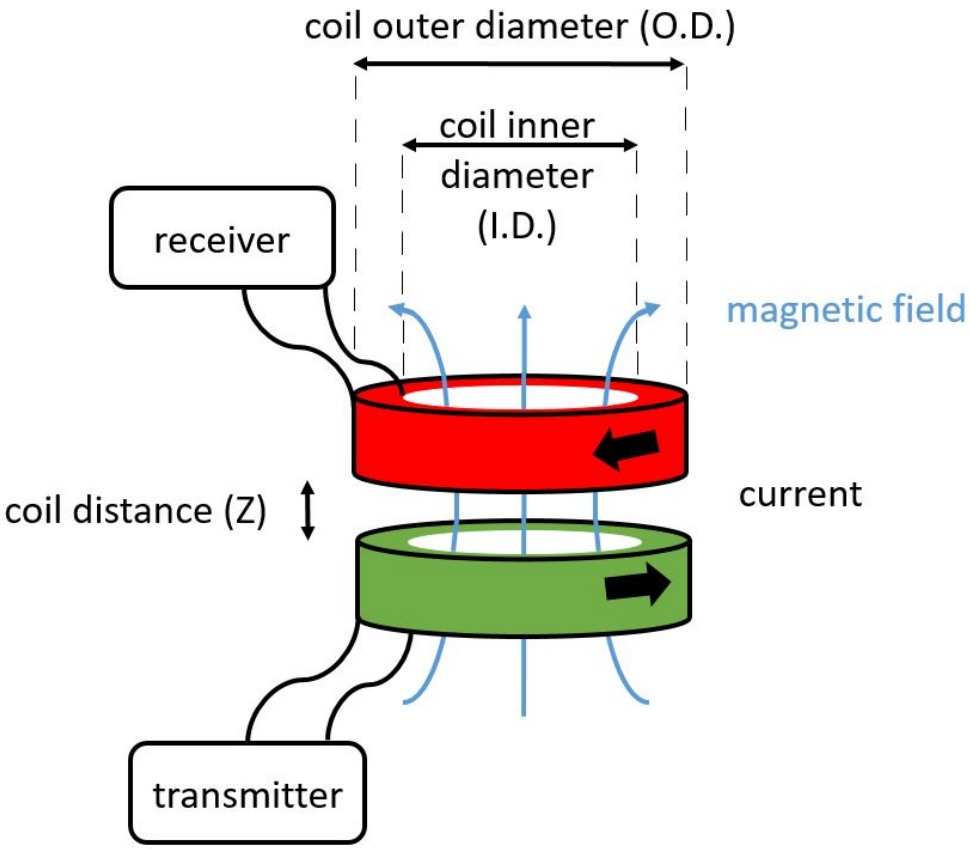

Figure 2.9: The fundamental physics of the coils.

The wireless power transfer takes place due to Faraday's law of induction, expressed mathematically in:

$$\Delta V = -N\frac{\Delta\phi}{\Delta t} \tag{2.1}$$

where V = voltage, N = number of coil turns, phi = magnetic flux and t = time. The law states that an electromotive force or voltage is induced by a change in the magnetic flux. The magnetic flux can be thought of as a water passing through a

screen, as seen in where the screen represents a closed body area or coil and the water mimics the effect of the magnetic field lines passing through the area. The magnetic flux has three dependencies that change the overall wireless power transfer. The first is the magnetic field, denoted by B in

$$\phi = |\vec{B}||\vec{A}|cos\theta. \tag{2.2}$$

The magnetic field is directly related to the magnetic flux. As the magnitude of the magnetic field increases, the magnetic flux increases proportionally. The area also is directly related to the magnetic flux, as the area of the coil increase so to does the magnetic flux. The final and most important aspect to the magnetic flux in the context of this work, is the relationship of the angle of the coil and the resulting change in magnetic flux. This angle change is something that significantly affects the overall output and efficiency of the wireless power transfer. As the angle increases or decreases from the 90°or perpendicular alignment of the coils, the magnetic flux decreases as less coil area is presented to the magnetic field. This characteristic plays an important role in the wireless power transfer and specifically the development of the near-field wireless power transfer modules and their use in the autonomous mobile microgrid[39][35]. The process of the wireless power transfer is similar to the way in which a transformer works, the primary coil receives alternating current voltage, creating a component of magnetic flux. Due to the proximity of the secondary coil to the primary coil, the magnetic field produced from the alternating current through

the primary coil induces an alternating current into the secondary coil. The inductive power transfer phenomenon occurs between two or more coils. In order for the process to occur the coupling coefficient (k) will fall within a range from 0 to 1. The coupling coefficient is based on the air gap between the primary and secondary coils. Because a transformer has a minimal air gap, the coupling coefficient is 0.95 and the transformer is said to be "strongly coupled". The near-field wireless power system has a coupling coefficient ranging from 0.01 to 0.5, thus the system is referred to as "weakly coupled" [40]. A generic example of an equivalent circuit for the primary and secondary of a wireless power system can be seen in Figure 2.10[41] and will be used to provide a generalized mathematical model found in the wireless power system. The input voltage or V_i is defined as

$$V_1 = I_1 R_1 - j\omega M I_2 \tag{2.3}$$

where I_1 and I_2 are the currents through the primary and secondary coils, R_1 is the resistance in the primary circuit, ω is the resonant frequency and M is the mutual inductance between the coils. From Figure 2.10, the output power P_0 can be described by

$$P_0 = I_2^2 R_L = ((\frac{\omega M I_1}{R_L + R_2})^2) R_L \tag{2.4}$$

where R_L represents the load resistance. The degree to which the coils are coupled

can be expressed by the coupling coefficient

$$k = \frac{M}{\sqrt{L_1 L_2}}. \tag{2.5}$$

In (2.5), M represents the mutual inductance of the two coils and L_1 and L_2 are the inductance values of the primary and secondary coil. The output power equation can now be updated to reflect the coupling coefficient as seen in

$$P_0 = ((\frac{\omega k \sqrt{L_1 L_2 I_1}}{R_L + R_2})^2) R_L \tag{2.6}$$

With the updated power out equation, it is imperative to have the power in, which is found with

$$P_i = I_1^2 R_1 + I_2^2 (R_2 + R_L). \tag{2.7}$$

Having both the P_0 and P_i allow the efficiency of the system to be calculated. The efficiency of the system in terms of the individual components in the equivalent circuit can be found by

$$\eta = \frac{P_0}{P_i} = \frac{R_L}{\frac{R_1 (R_L + R_2)^2}{k^2 \omega^2 L_1 L_2} + R_L + R_2}. \tag{2.8}$$

The previous equation shows that the coupling coefficient, k, plays a vital role in the wireless power transfer.

As mentioned previously, the near-field wireless system is comprised of two separate modules (Figures 2.11, 2.12, and 2.13).Specific to this work, the primary module, or

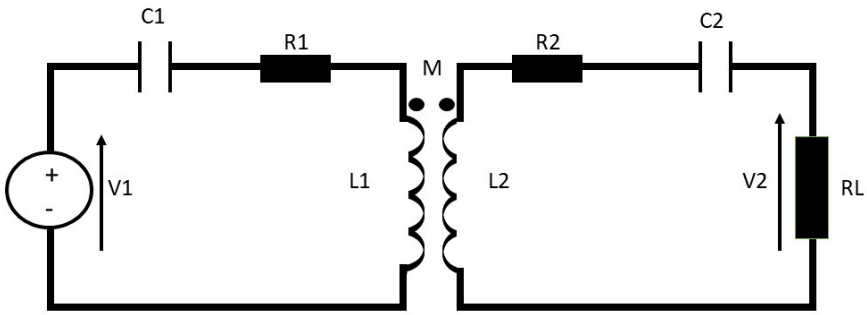

Figure 2.10: Equivalent wireless power circuit diagram.

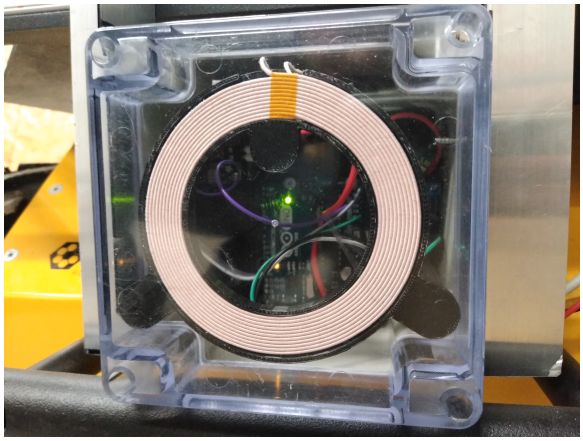

Figure 2.11: Primary coil hardware is mounted on the front of the Husky UGV

the transmitting module, is mounted to the Husky UGV. The transmitting module consists of a 1.3 mm Litz wire coil with an inner diameter of 70 mm and an outer diameter of 88 mm. While the receiving module also utilizes 1.3 mm Litz wire, the secondary coil has an inner coil diameter of 70 mm and an outer coil diameter of 83 mm. The UGV system supplies the transmitting module with a regulated direct current voltage, which is inverted to provide power to the transmitting coil. The alternating current induced onto the receiving coil is then rectified to provide direct current power to the load.

Figure 2.12: Secondary wireless power receivers are mounted to demonstration loads.

Because the two modules are electrically isolated, wireless power systems can provide safe and reliable operation in extreme environments. This is one of the benefits of wireless power systems and why they are considered an ideal solution for charging electric vehicle batteries. In smart grid applications, EV can be used as load or as distributed power resources in a concept known as vehicle-to-grid (V2G) operation [42][43]

Chapter 3 presents the hardware and software utilized in the wireless power transfer system as well as the development of the autonomous mobile docking control system used to guide the agent during wireless power transfer. Further,the experimentation

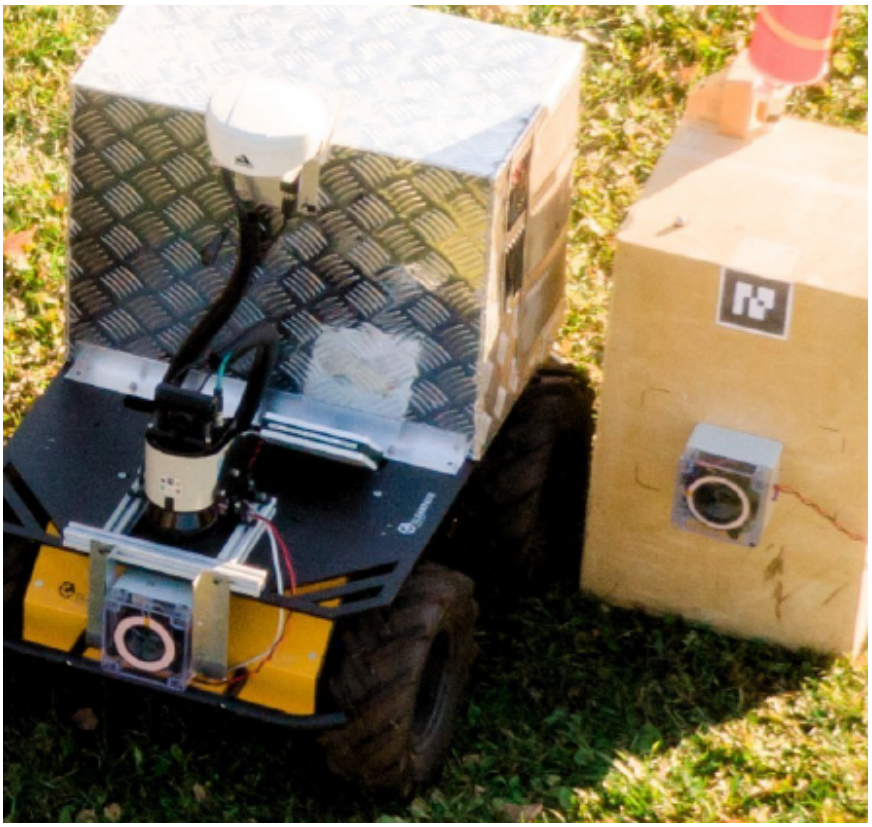

Figure 2.13: Near field wireless modules mounted on Husky UGV and stationary load.

used in the development of these system is explored at length.

Chapter 3

Hardware and Software Implementation

3.1 Introduction

This chapter provides information on the wireless power transfer hardware and software implemented on the autonomous mobile micro-grid created by the research team. Evolution of the system due to environmental and terrain changes is also discussed. Within this project, two different hardware and software setups were used in order to cater to the evolving scope of work. Both systems will be discussed in detail. To conclude this chapter, the wireless power transfer systems docking control method is

also described f[1].

3.2 COTS Hardware Selection

To achieve the project goals, the team needed to monitor the voltage, current, and power of the primary and secondary modules. The first step was to decide how to collect the required data, while keeping the project parameters in mind. There are many different commercial off the shelf (COTS) pieces of hardware that were capable of performing the desired task. A very popular device, and the one used in this work, is the Arduino UNO [44][45]. The Arduino UNO is built upon the ATmega328, which is a single-chip 8-bit microprocessor. Atmel developed the ATmega328 as a low-powered, low-cost unit that has since been used widely in various types of automation and control systems. Another advantage of implementing the Arduino UNO micro-controller was the research team's familiarity with the Arduino's Integrated Development Environment or IDE. The IDE provides the user with a straight forward programming interface to upload code to the Arduino UNO via the USB connection. The unit utilizes a language that is derived from a combination of C and C++, which again was something that was viewed as a positive attribute when implementing into the near-field wireless system. The Arduino UNO contains 14 digital pins, 6 analog inputs, USB connection, In-Circuit Serial Programming or ICSP header,and a 16

[1]The material in this chapter is reprinted in majority from [16]

MHz quartz crystal. The unit can be powered from a DC source via the USB jack or barrel jack connection [46]. To measure the voltage and current, an Adafruit breakout board was used [47]. The module used is equipped with an INA219 microchip, an integrated circuit (IC) design introduced by Texas Instrument. The zero-drift, bi-directional device measures the voltage drop across the surface mounted 100 ohm shunt resistor. This configuration allows for the measurement of current, voltage and power in various embedded circuits. What made the Adafruit INA219 breakout board invaluable to the near-field wireless power application was the Inter-Integrated Circuit Protocol or I2C ability of the module. The I2C capability would allow for multiple components and addressing, which played a key role in the evolution of the autonomous micro-grid. The I2C bus consists of a serial data pin (SDA) and serial clock pin (SCL) which provide communication of data and between the module and the micro-controller. As stated earlier, the Adafruit INA219 device is outfitted with a 0.1 W shunt resistor (2 W), accurate to +/-1 and 12-bit A/D converter. The unit has a detection range of 3.2 A and a resolution of 0.8 mA. The breakout board also provided adequate computation capability with a response time of 68 milliseconds.

Combination of the Adafruit sensor and Arduino micro-controller allowed for measurements and computation of the power being transferred from the primary module, in addition to the power being consumed by the secondary module's DC load circuit. Since the primary module was mounted to the UGV, the existing USB network connection and I2C communication protocol provided the raw data directly to the

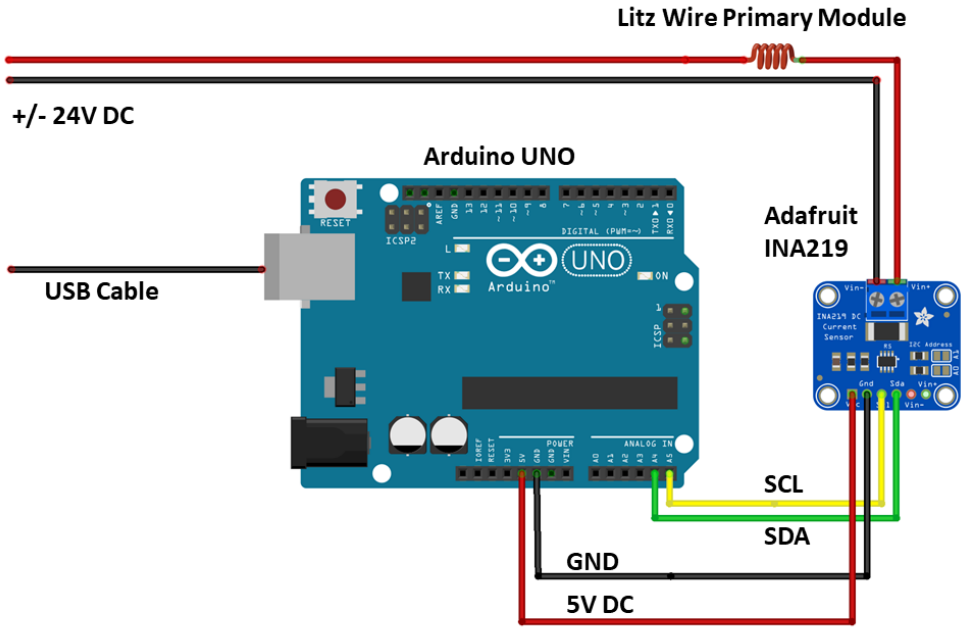

Figure 3.1: The primary side hardware is comprised of a litz wire coil module, Arduino micro-controller, and Adafruit current sensor.

Robotic Operating System (ROS) that controls the UGV. The code that was created to operate the Adafruit INA219 chip is shown in A.2. This code was written to monitor the voltage, current and overall power that is produced by the primary near-field wireless module. This code was loaded onto the Arduino UNO housed on the UGV genset agent. Figure 3.1 is a circuit diagram of the setup on the mobile genset UGV. The Arduino UNO, Adafruit INA219 and Litz-wire primary side coil are shown in Figure 3.2. These components combined form the primary side of the near-field wireless module as seen in Figure 2.11.

The secondary module of the near-field wireless power transfer system required a different setup than that of the primary module. This change was due to the secondary

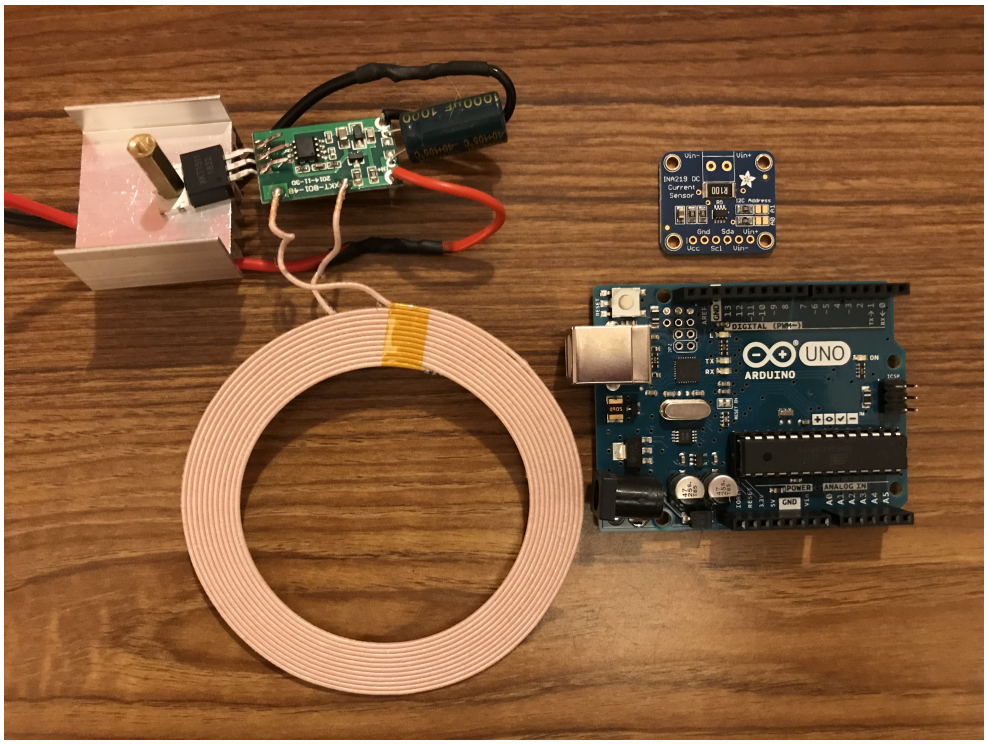

Figure 3.2: The primary side hardware is comprised of a Litz wire coil module, Arduino micro-controller, and Adafruit current sensor.

modules non-networked location. Since the secondary module was mounted to a stand-alone load, the data from the secondary module did not have a live connection to ROS that the primary module capitalized on.

To collect the desired data from the secondary module load circuit, an Adafruit data logging shield was added to an Arduino UNO micro-controller. The unit can write data to a secure digital (SD) memory card in 16 or 32 bit file allocation table (FAT16 or FAT32) format providing up to 32 gigabits of readable data. In A.3, the code used for the Arduino UNO and Adafruit data logging shield contained in the secondary near-field wireless module mounted on the fixed load is found. This

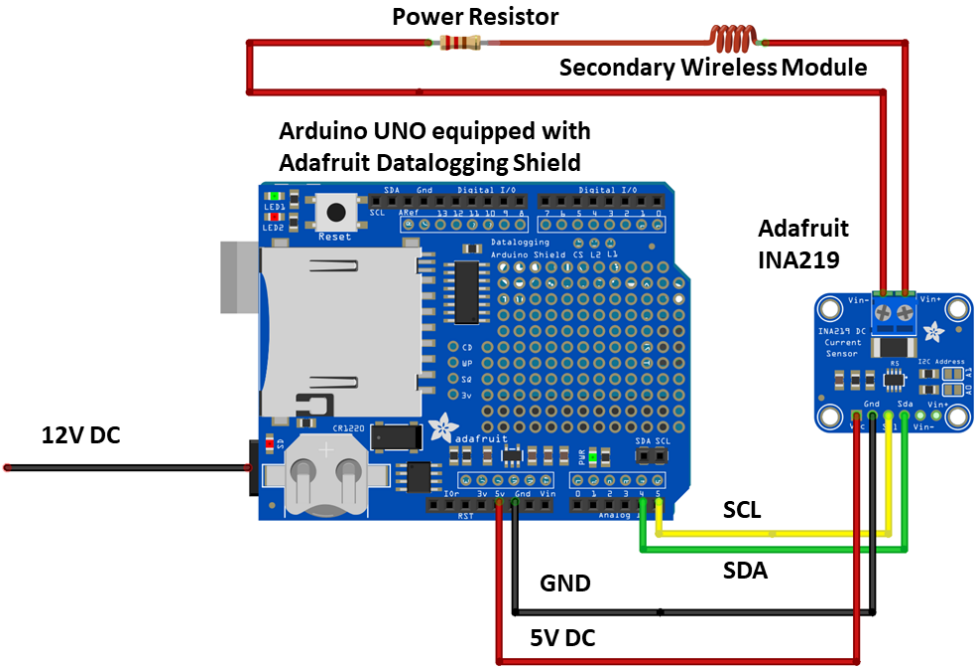

Figure 3.3: The secondary side hardware is comprised of a litz wire coil module, Arduino micro-controller, Adafruit datalogging shield and a Adafruit current sensor.

code also made use of the Adafruit INA219 breakout board to monitor the voltage, current and power at the load. The difference with the code in A.3 to that found in A.2 has to do with the requirement of a real time clock or RTC. This data shield includes a real time clock or RTC, allowing for synchronization of time signatures of the primary and secondary module data. This time stamp would allow for greater precision during post-processing of the near-field wireless transfer data. The Arduino that was mounted to the mobile bus agent did not require an RTC as it was linked to the HUSKY onboard computer which was in direct communication with ROS. The hardware used in these systems is shown in Figures 3.2 and 3.4. A schematic of the system can be seen in Figure 3.3.

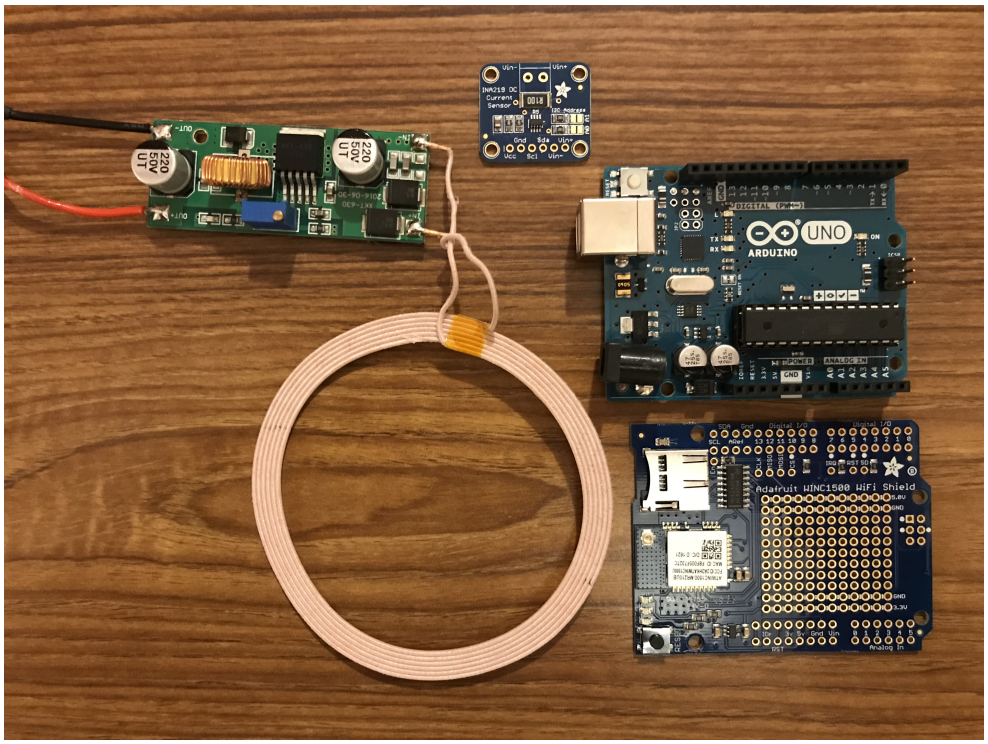

Figure 3.4: The secondary side hardware is comprised of a litz wire coil module, Arduino micro-controller, Adafruit data shield, and Adafruit current sensor.

The primary and secondary near-field wireless modules were originally housed in a plastic storage container mounted to the front of the UGV, as seen in Figure 3.5. This original prototype was later exchanged for an enclosure capable of containing the wireless power modules, micro-controllers, and appropriate sensor array. The system needed to be robust to handle the abusive nature of autonomous docking and traversal in an outdoor environment. The calibration period of the docking controller proved that the system was adequate and held up to the inadvertent and repetitive collisions between the mobile bus agent containing the near-field wireless primary module and the near-field wireless secondary module contained on the fixed load. Rather than using adhesives to contain the hardware within the enclosure, a 3D printer was used

Figure 3.5: Prototype of Near-field Wireless Power System.

Figure 3.6: 3D printed Litz wire support ring.

to create novel brackets to arrange the components. Two 3D-printed components were created (Figures 3.6 and 3.7) and can be assembled to create the bracket seen in Figure 3.8.

Figure 3.7: 3D printed micro-controller enclosure base.

3.3 System Overview

The primary side module is controlled via an Arduino UNO unit that also monitors the primary module's performance, providing real-time power and efficiency information. The secondary module also incorporates an Arduino UNO controller, paired with a data logging shield. This setup allows for the analysis of both systems' performance on the secondary side of the connection, which can then be utilized for further load analysis. The primary side module system data is fed into ROS on the Husky robot to provide real-time data to the operator.

The primary module requires a $24V$ and $1A$ regulated direct current supply, which

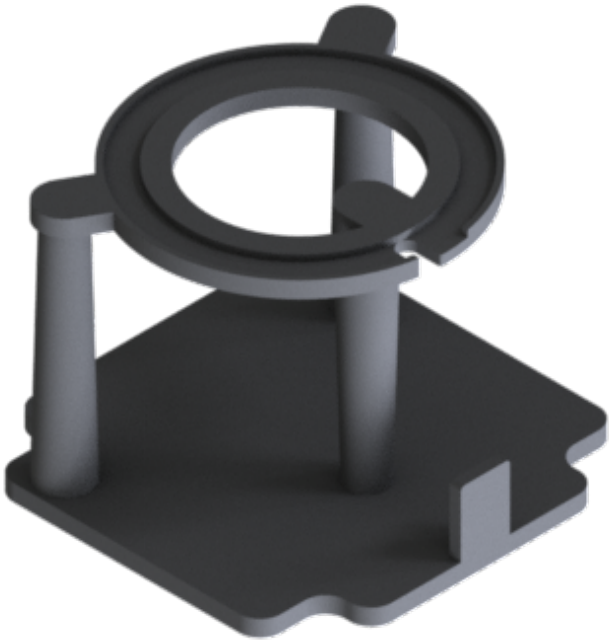

Figure 3.8: 3D printed Near-field wireless power transfer mount system.

is provided by the Husky UGV. The secondary module is capable of delivering direct current at $12V$ and $2A$. A front-mounted design (as seen in Figure 2.4) was chosen to simplify control and target acquisition.

3.4 Docking Controller

The need for mobile UGVs to have highly accurate relative positioning data is paramount for successful near-field wireless docking. The docking controller requires localization data from an external source through a constant feed, in this case, the data is acquired via various sensors including; a global positioning system (GPS), attitude heading and reference system (AHRS), 2-D LiDAR, wheel encoder odometry,

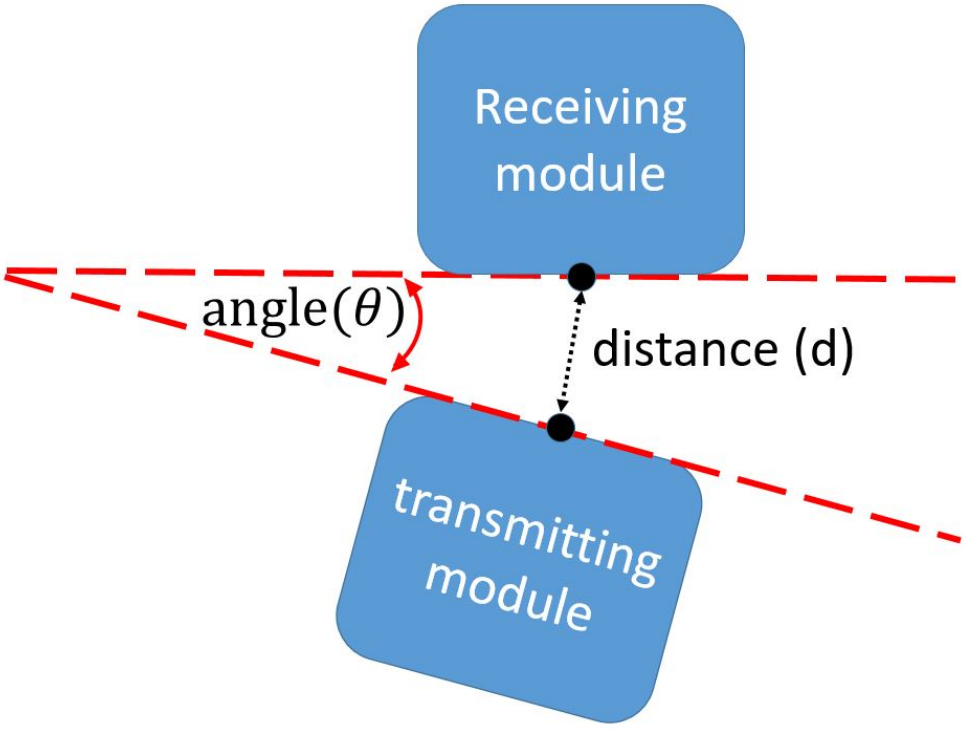

Figure 3.9: Transmitter and receiver modules represented in the angle and distance domain.

and visual camera referencing.

The UGV initially begins at a datum point pre-loaded into the system. From this datum point, the UGV traverses to the rendezvous way-point using GPS, AHRS, 2-LiDAR, and odometry data. Once the UGV reaches the rendezvous point, the camera activates to confirm if the augmented reality (AR) marker, located on the target, is within the visual frame of the camera. The controller then pans the UGV, allowing the fixed camera to search for the AR marker. Upon target acquisition, the controller computes an ”x”,”y”,” theta” docking pose in reference to the AR marker (Figure 3.7 shows a representation of this calculated space).

This docking pose is then used as the final docking way-point goal. The UGV then visually "servos" - a process in which the fixed camera on the UGV locks onto the AR marker and guides the UGV to the final docking position. Once at the final calculated docking position, the controller interprets the data from the near-field wireless power modules' sensors to assist in determining docking success. The minimum limits for docking success were determined from the initial power transfer characterization and can be seen in Table 1. If the docking pose error is greater than the pre-set parameters, the controller initiates the re-docking procedure, which returns the UGV to the docking way-point to repeat the final docking sequence. The controller then implements a proportional feedback loop in the visual servo mode to obtain the final pose. If the docking attempt is deemed successful, the controller indicates success and notifies the operator. A block diagram of the decision process of the docking controller is shown in Figure 3.10 and the code developed for the mobile bus agent is found in A.1.

3.5 Enhanced Hardware

The design of the near field wireless power system was later changed to incorporate updated hardware. Additional research found that there were various systems that could provide real-time feedback [48][49][50]The upgraded components allow for real-time feedback from the secondary modules. Feedback from the loads provided

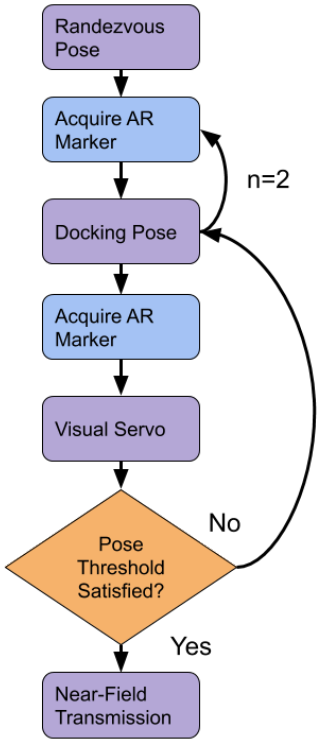

Figure 3.10: Docking control for wireless power transfer depends on both canonical elements of the ROS move_base software, and custom algorithms.

additional data, allowing for various development of the micro-grid system.

The limited options available to provide wireless communication from the secondary modules in real-time proved to be challenging. There were three off-the-shelf technologies that could be implemented into the system with varying degrees of difficulty: Bluetooth, FM radio transmission, and WiFi. The team first experimented with an Adafruit ATWINC1500 WiFi shield, which would utilize the existing Arduino hardware and software that was in place; however, the Arduino Uno was incapable of the computational speed required by ROS. There was initial success using the Adafruit ATWINC1500 WiFi shields on an Arduino Mega, and the team considered using this

piece of hardware for further development. However, the large size of the Arduino Mega would require significant design changes as it simply did not fit into the existing project enclosures, thus resulting in further 3D-printing and updated enclosures.

Next, experimentation was conducted using the Adafruit HUZZAH32 ESP32 Feather board and the Adafruit Feather HUZZAH ESP8266 breakout board. Both boards have a 32-bit processor which would provide plenty of computation power; however, the ESP32 has a dual-core CPU providing 160MHz to 240MHz. The the ESP8266 utilizes a single-core processor that operates at 80MHz. The benefit of either of these devices is that they were both could be programmed using the Arduino IDE based of the C/C++ programming language. Each unit had the ability to utilize the existing Adafruit INA219 boards that were used to monitor the voltage, current and power at load. Both options would provide adequate communication and the ability to be powered by a small lithium ion power source concealed safely within the modules enclosure. The code that was developed to operate these devices can be found in A.4 and A.5 Ultimately, the Adafruit Feather HUZZAH ESP8266 breakout board was easier to work with and chosen as the platform for further development [51]. By substituting the Arduino micro-controllers with an Adafruit Feather HUZZAH ESP8266 breakout board, the team achieved real-time feedback from the load, all while maintaining the original primary and secondary modules' design. This new hardware would provide the ability to charge the wireless sensor network and associated lithium ion battery

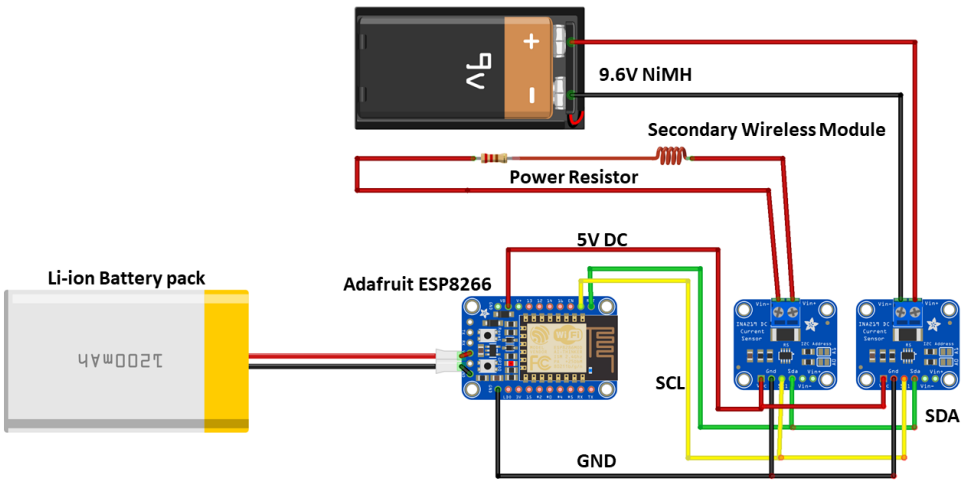

Figure 3.11: The updated secondary side hardware is comprised of a litz wire coil module, ESP8266 micro-controller and two Adafruit current sensors.

packs on the loads[23][52]. Additionally, the Adafruit Feather HUZZAH ESP8266 allowed the team to continue development using the same software as the Arduino IDE and saved the research group a significant amount of time during mission deployment. The updated hardware can be seen in Figure 3.11.

Chapter 4

Experimental Results

4.1 Introduction

This chapter provides information on the autonomous mobile micro-grid wireless power transfer experimental results. Details on the power output and docking controller success rates are examined and statistical methods applied to quantify the results f[1].

[1]The material in this chapter is reprinted in majority from [16]

4.2 Results

The objective of this research was to power a micro-grid load via near-field wireless power, while monitoring the power and efficiency of the system. It was important to characterize the relationship of the primary module to the secondary module and demonstrate that the data acquisition system does, in fact, show that the inverse-square law holds true for the electromagnetic field produced by the primary module.

Power data from the primary and secondary modules at various alignments was collected and used to analyze the system's performance. Diverse alignments, with a set resistive load, was used to characterize the relationship of the transmitted power to the received power as a function of distance and angle.

The load was chosen to represent a realistic application of the near-field power system. A 7 Ω power resistor, connected across the receiving modules output contacts, was utilized to create a potential constant current draw of approximately 1.7 A and a power output of approximately 20 W. The resistive load allowed the circuit to remain within the range of the rated output of the system, while simultaneously allowing output validation of the hardware setup and data acquisition. By isolating the distance and angle between the two modules, these variables became the determining factor in the power output and overall efficiency of the system. With the current system

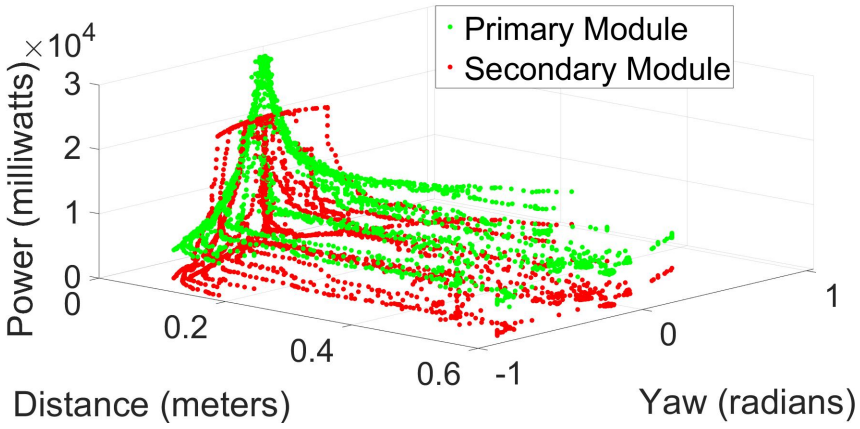

Figure 4.1: Power relationship between the primary and secondary coils as a function of absolute distance and angle between the faces of the enclosures.

configuration, pre-calculated estimates of current draw and power output at the load were replicated. The near-field wireless system performed admirably and produced power transfers at distances and angles greater than expected. The power output of the primary and secondary modules compared to the varying distances and varying yaw between the modules is demonstrated in Figure 4.1.

A two-dimensional representation of the power output of the modules in relation to the distance space can be seen in Figure 4.2. Figure 4.3 shows the power output of the modules with respect to the yaw or the z-axis. From Figures 4.2 and 4.3, we observe that with a 7 Ω load in place, we can experimentally draw our calculated power of 20 W.

It was concluded that to achieve a quantitative quality power transfer, one would need to use the power transfer characterization data to set distance and angle limits. These limits (or thresholds) would either determine docking success or initiate

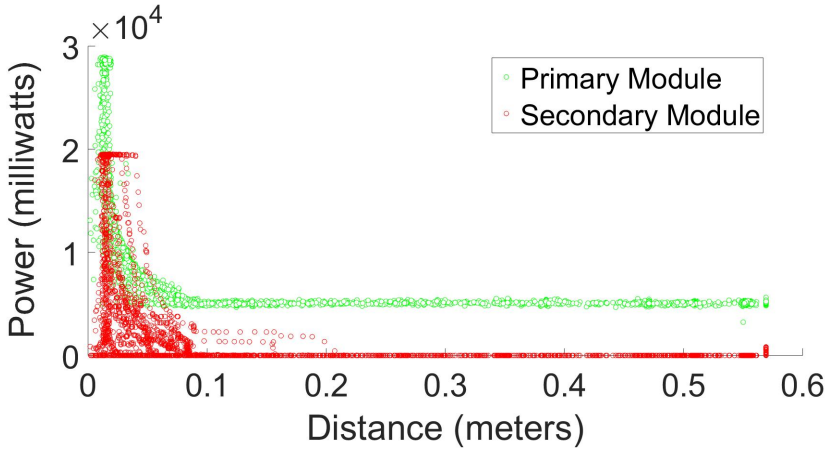

Figure 4.2: Correlation of the distance between the faces of the Primary and Secondary modules and the power transferred.

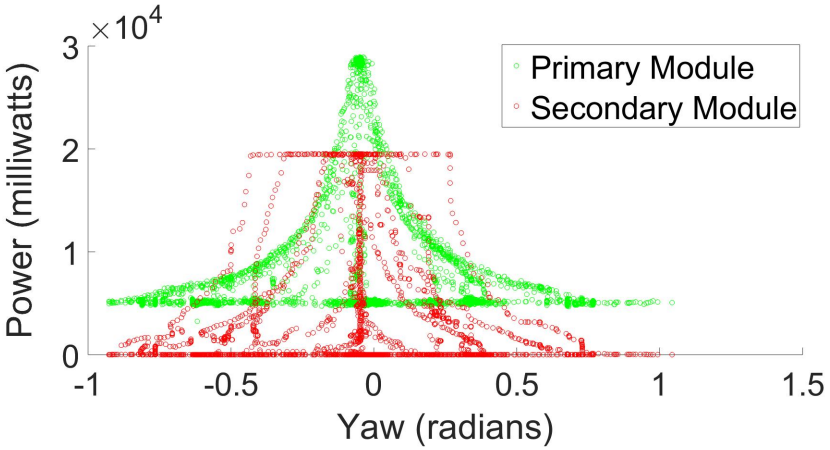

Figure 4.3: Correlation of the yaw and the power transferred between the primary and secondary modules.

the re-docking sequence. The empirically chosen scalar distance and absolute angle parameters determined from the initial power transfer characterization data were determined to be 0.015 meters and +/- 0.625 radians.

The efficiency of the system was also of interest during data collection. Using the

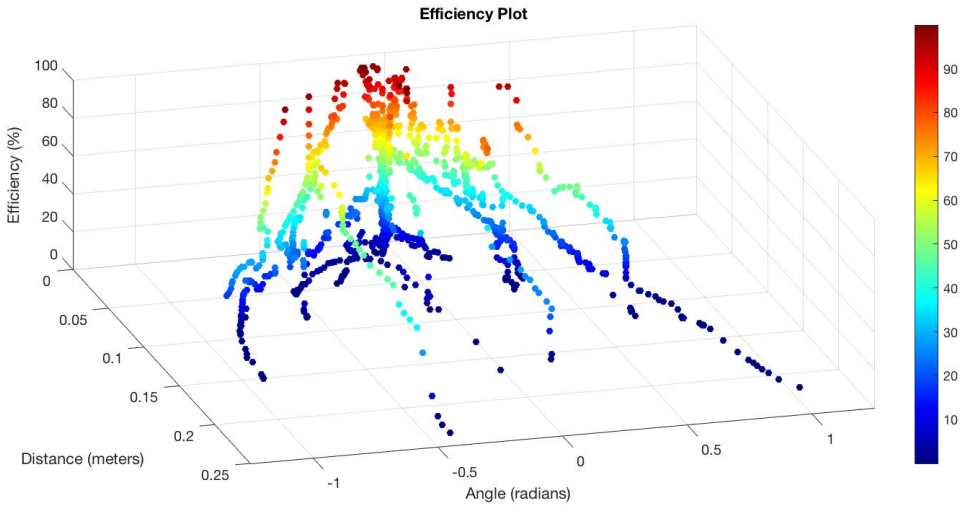

Figure 4.4: Plot of efficiency of near-field system.

power, distance, and angle data collected from both the primary and secondary modules, a 3-dimensional plot of the efficiency of the system was created (Figure 4.4). System performance greater than 60% capacity was also achieved within the distance and angle space chosen as our docking threshold parameters from Table 4.1 (Figure 4.4).

Further experimentation was conducted to confirm that the distance and angle recorded by the hardware mounted to the Husky, and disseminated by the ROS, was accurate. First, a 60-degree grid, determined by using the minimum and maximum docking angle while still providing observable wireless power transfer, was marked on the floor of the lab. The range was 60-120 degrees, with 90 degrees representing a flush alignment of the modules. Wireless power transfer measurements were then recorded at 10-degree increments over the 60-degree range and at increasing distances

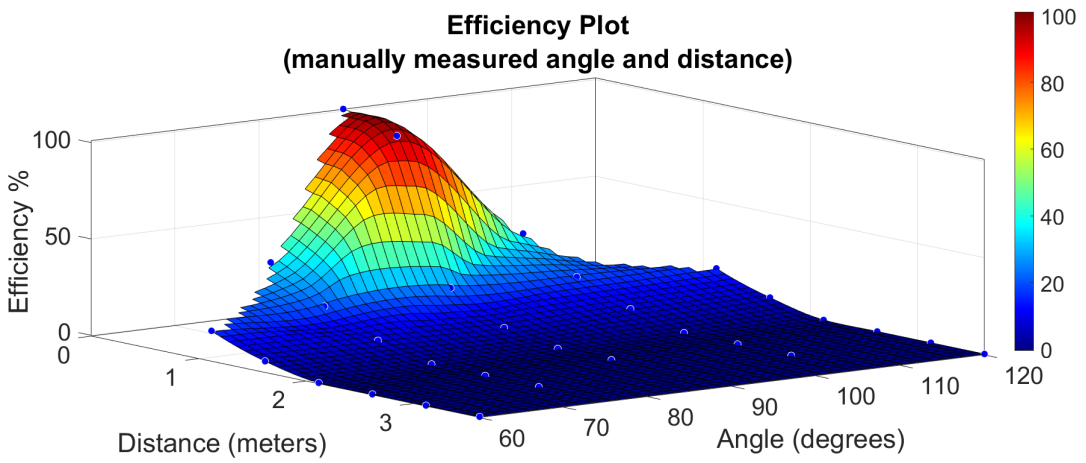

Figure 4.5: Efficiency data using manual measurement of the distance and angles between the faces of the Primary and Secondary modules.

between the primary and secondary modules. The next step was to manually move the load through a range of hand-placed measurements while recording the power transfer data at the predetermined points. To maintain replicability, the same 7 Ω power resistor was again connected across the receiving modules' output contacts, creating a current draw of approximately 1.7 A and power output of approximately 20 W. The distance and angle were observed by the method mentioned above, while the power data was recorded by hand using a multi-meter. These results are graphically conveyed in Figure 4.5.

During the experiment, the Husky's sensor array also recorded the distance and angle of each predetermined point. The Husky data interpreted by the ROS was then used to create a graphical representation similar to the manually recorded data, which can be seen in Figure 4.6.

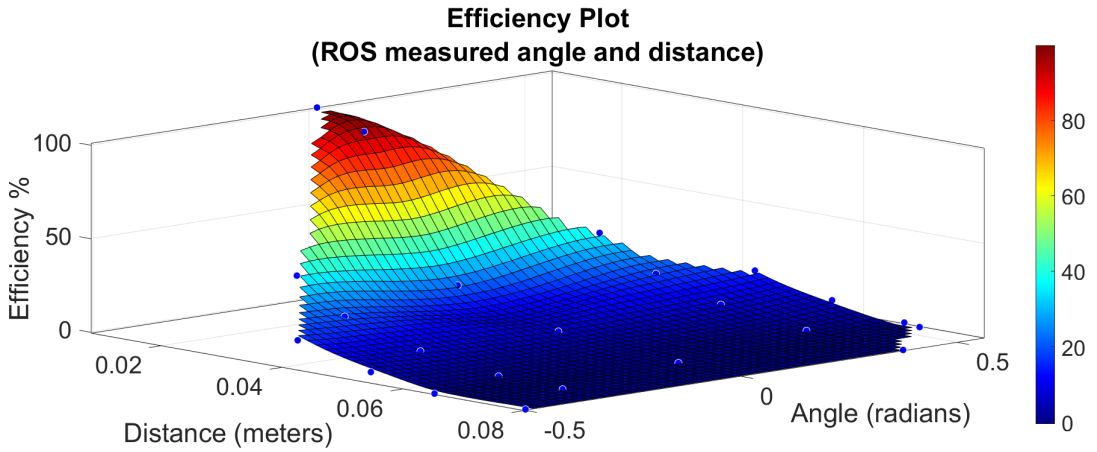

Figure 4.6: Efficiency data using ROS measurement of the distance and angles between the faces of the Primary and Secondary modules.

To provide a statistical analysis of the system, the relationship between the primary and secondary power output data was calculated using the Pearson Correlation Coefficient shown in

$$\rho(A,B) = \frac{cov(A,B)}{\sigma_A \sigma_B}. \tag{4.1}$$

The co-variance of A and B is found from

$$cov(A,B) = \frac{1}{N-1}\sum_{i=1}^{N}(A_i - \mu_A)^*(B_i - \mu_B). \tag{4.2}$$

The standard deviation of the primary and secondary output power are σ_A and σ_B, respectively and * denotes the complex conjugate [53][54].

The correlation coefficient was calculated using MATLAB and found to be 0.7739. A correlation coefficient value can range from -1 to 1, with -1 representing a direct negative correlation, zero representing no correlation, and 1 characterizing a direct

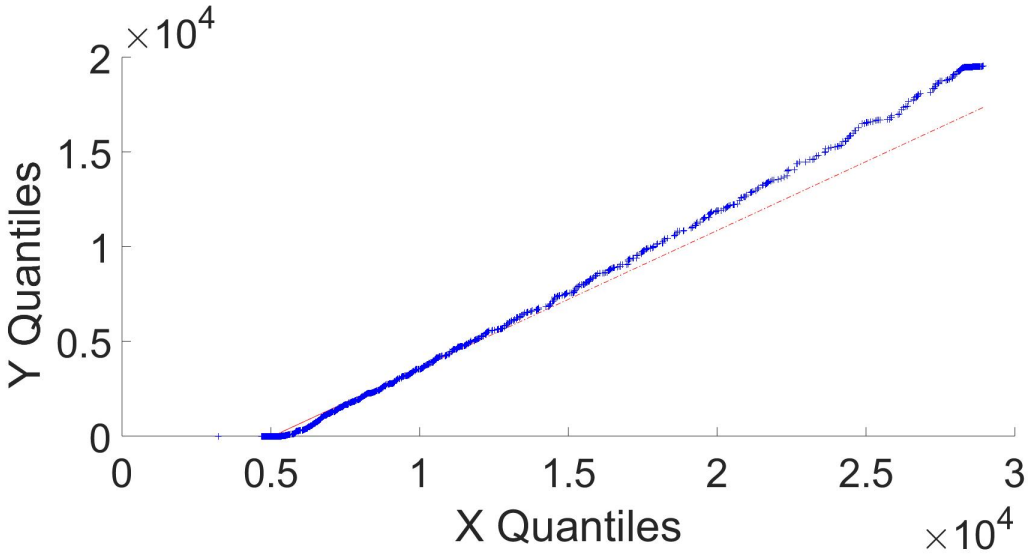

Figure 4.7: Quantile-Quantile Plot of the Primary and Secondary module output power.

positive correlation. Therefore, these results show a positive correlation trend of the primary and secondary power output data.

In addition to calculating the correlation coefficient, a quantile-quantile plot (Figure 4.7) was also created as a means to graphically compare the probability distribution of the primary and secondary power output data. In comparing the two quantile data sets of the output power of each module, a linear trend in observed, suggesting the data is normally distributed [55].

The near-field wireless Husky UGV, in the current setup of using wheel odometry and camera visualization only, demonstrated that an 80% docking success rate can be achieved in an indoor environment. A graphical representation of the docking trajectory and success rate can be seen in Figure 4.8. The blue lines represent successful

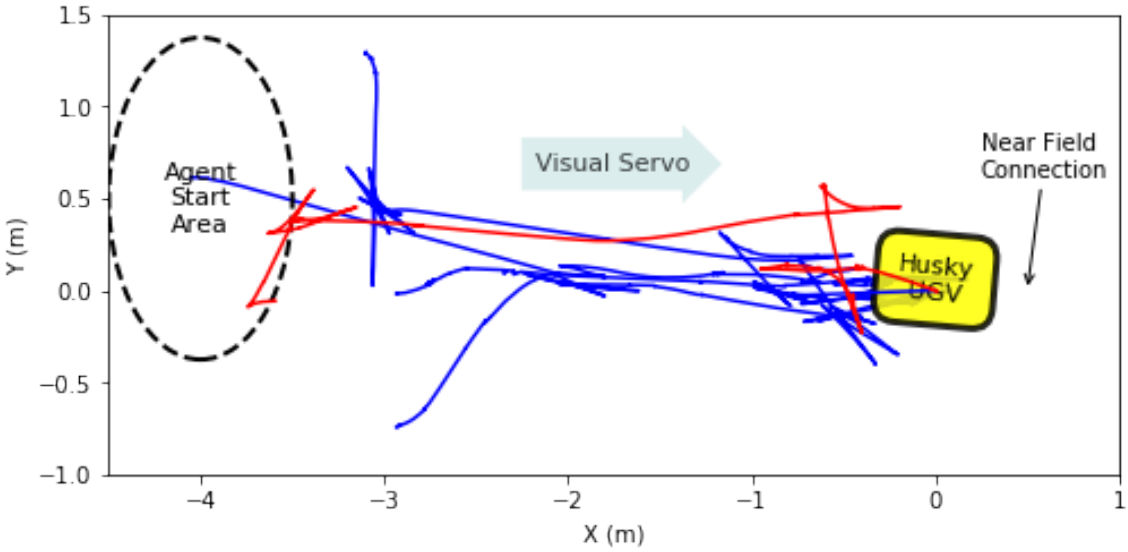

Figure 4.8: Docking trajectory attempts represented from wheel odometry and camera visualization data.

docking trajectories while the red line represents docking failure. With use of the entire UGV sensor network in an outdoor environment, the Husky UGV can achieve a 73% docking success rate.

4.3 Discussion

When implemented, the power output of the modules was within the range of the calculated values. An output of 20 W from our secondary module allowed for utilization of the near-field wireless power transfer system in the micro-grid to provide load support and system optimization.

The use of camera visualization as feedback for the docking controller yielded an

80% success rate. Also taken into consideration, was that this UGV docking took place in a two-dimensional environment. In other words, this work was conducted on relatively flat surfaces, void of elevation changes. The 80% success rate can be improved upon by replacing the fixed mount of the modules with one that would allow yaw on the vertical access. If determined that higher precision is needed, a gimbal system allowing roll, pitch, and yaw could also be implemented. The 80% success rate was also achieved using a 180-degree area, oriented outward from the load. Reduction of this area to 160 degrees was observed to improve the success rate to 93%. Based on the results of this experimentation, the research team was able to provide wireless power transfer using camera visualization as feedback control at success rates of 80% - 93%.

Chapter 5

Conclusion and Future Work

5.1 Conclusion

The statistical analysis and data collection demonstrated that by characterizing the relationship between the transmitting module and secondary module, an accurate docking controller can be implemented using camera visualization. With the current design, the system provides an opportunity to scale-up and increase the power transfer capability without drastic design changes to the system.

5.2 Future Work

Continued development and data trials are anticipated with this project. Advancement in the UGV cabling agent could increase the utility of the autonomous mobile micro-grid. Plans for the near-field wireless system include; larger scale power transfer between the modules, increased docking precision from advanced sensor equipment, mission planning optimization, and the use of live feedback from the load module hardware to assist in docking. The advancements in hardware and software pave the way for additional contributions toward the advancement of the autonomous mobile micro-grid and near-field wireless power transfer systems.

References

[1] "Edison's electric light and power system," accessed 03-01-2022. [Online]. Available: https://ethw.org/Edison's_Electric_Light_and_Power_System

[2] W. W. Weaver, N. Mahmoudian, and G. Parker, "Autonomous mobile power blocks for prepositioned power conversion and distribution," in *TARDEC Ground Vehicle Systems Engineering and Technology Symposium*, 2012.

[3] B. Moridian, N. Mahmoudian, W. W. Weaver, and R. D. Robinett, "Robotic power distribution system for post-disaster operations," in *International Symposium on Safety, Security, and Rescue Robotics*. IEEE, 2015, pp. 1–6.

[4] G. Cave, W. Goodwin, M. Harrison, A. Sadiq, and T. Tryfonas, "Design of a sustainable forward operating base," in *International Conference on System of Systems Engineering*, 2011, pp. 251–257.

[5] "Hybrid generator would cut military base fuel costs in half earl energy attaches lithium-ion batteries to off-grid generators in u.s. defense department

contract," accessed 03-01-2022. [Online]. Available: https://spectrum.ieee.org/hybrid-generator-would-cut-military-base-fuel-costs-in-half

[6] "Strategy charts path to fuel-efficient forward operating base," accessed 03-01-2022. [Online]. Available: https://www.army.mil/article/157524/strategy_charts_path_to_fuel_efficient_forward_operating_base

[7] "Lunar living: Nasa's artemis base camp concept," accessed 03-01-2022. [Online]. Available: https://blogs.nasa.gov/artemis/2020/10/28/lunar-living-nasas-artemis-base-camp-concept/

[8] B. Moridian, D. Bennett, N. Mahmoudian, R. Robinett, and W. W. Weaver, "Design of Mobile Microgrid's Hierarchy for Power Distribution," *ASME Dynamic Systems and Control Conference*, vol. 3, Oct. 2015.

[9] B. Moridian, N. Mahmoudian, W. W. Weaver, and R. D. Robinett, "Postdisaster Electric Power Recovery Using Autonomous Vehicles," *IEEE Transactions on Automation Science and Engineering*, vol. 14, no. 1, pp. 62–72, Jan. 2017.

[10] J. Larson, M. Bruch, and J. Ebken, "Autonomous navigation and obstacle avoidance for unmanned surface vehicles," in *Unmanned Systems Technology VIII*, vol. 6230. International Society for Optics and Photonics, 2006, p. 623007.

[11] A. Elfasakhany, E. Yanez, K. Baylon, and R. Salgado, "Design and development of a competitive low-cost robot arm with four degrees of freedom," *Modern Mechanical Engineering*, vol. 1, no. 02, p. 47, 2011.

[12] L. Olvitz, D. Vinko, and T. Švedek, "Wireless power transfer for mobile phone charging device," in *International Convention MIPRO*. IEEE, 2012, pp. 141–145.

[13] J.-Y. Lee and B.-M. Han, "A bidirectional wireless power transfer ev charger using self-resonant pwm," *IEEE Transactions on Power Electronics*, vol. 30, no. 4, pp. 1784–1787, 2015.

[14] F. Musavi and W. Eberle, "Overview of wireless power transfer technologies for electric vehicle battery charging," *IET Power Electronics*, vol. 7, no. 1, pp. 60–66, 2014.

[15] C.-S. Wang, O. H. Stielau, and G. A. Covic, "Design considerations for a contactless electric vehicle battery charger," *IEEE Transactions on industrial electronics*, vol. 52, no. 5, pp. 1308–1314, 2005.

[16] C. Greene, J. Naglak, C. Majhor, J. P. Bos, and W. W. Weaver, "Near field wireless power transfer via robotic feedback control," in *IEEE Aerospace Conference*, 2020, pp. 1–7.

[17] B. Moridian, N. Mahmoudian, W. W. Weaver, and R. D. Robinett, "Postdisaster electric power recovery using autonomous vehicles," *IEEE Transactions on Automation Science and Engineering*, vol. 14, no. 1, pp. 62–72, Jan 2017.

[18] A. Talukder, A. Panangadan, T. Herrington, A. Blumberg, and N. Georgias,

"Autonomous adaptive resource management in sensor network systems for environmental monitoring," in *IEEE Aerospace Conference*, March 2008, pp. 1–9.

[19] S. A. Darani, C. D. Majhor, W. W. Weaver, R. D. Robinett, and O. Abdelkhalik, "Optimal positioning of energy assets in autonomous robotic microgrids for power restoration," *IEEE Transactions on Industrial Informatics*, vol. 15, no. 7, Jul. 2019.

[20] J. Naglak, C. Greene, C. Majhor, N. Spike, J. P. Bos, and W. W. Weaver, "Autonomous power grid formation for surface assets using multiple unmanned ground vehicles," in *IEEE Aerospace Conference*. IEEE, 2020, pp. 1–8.

[21] C. D. Majhor, J. E. Naglak, C. S. Greene, W. W. Weaver, and J. P. Bos, "Recharging of distributed loads via schedule optimization with autonomous mobile energy assets," in *IEEE Aerospace Conference*. IEEE, 2020, pp. 1–9.

[22] J. Johnson, E. Basha, and C. Detweiler, "Charge selection algorithms for maximizing sensor network life with uav-based limited wireless recharging," in *IEEE Conference on Intelligent Sensors, Sensor Networks and Information Processing*, April 2013, pp. 159–164.

[23] C. M. Angelopoulos, S. Nikoletseas, and T. P. Raptis, "Efficient wireless recharging in sensor networks," in *IEEE International Conference on Distributed Computing in Sensor Systems*, May 2013, pp. 298–300.

[24] L. Li, X. Yixiang, H. Xiaoguang, D. Haibin, Z. Hanyu, C. Jun, and L. Jin, "A new rechargeable wsns based multi-uavs network and topology control algorithm," in *IEEE Conference on Industrial Electronics and Applications*, June 2015, pp. 507–512.

[25] S. Chitta, E. Marder-Eppstein, W. Meeussen, V. Pradeep, A. Rodríguez Tsouroukdissian, J. Bohren, D. Coleman, B. Magyar, G. Raiola, M. Lüdtke, and E. Fernandez Perdomo, "ros_control: A generic and simple control framework for ROS," *The Journal of Open Source Software*, vol. 2, no. 20, p. 456, Dec. 2017. [Online]. Available: http://joss.theoj.org/papers/10.21105/joss.00456

[26] W. C. Brown, "The history of wireless power transmission," *Solar energy*, vol. 56, no. 1, pp. 3–21, 1996.

[27] J. Garnica, R. A. Chinga, and J. Lin, "Wireless power transmission: From far field to near field," *Proceedings of the IEEE*, vol. 101, no. 6, pp. 1321–1331, 2013.

[28] N. Shinohara, "The wireless power transmission: inductive coupling, radio wave, and resonance coupling," *Wiley Interdisciplinary Reviews: Energy and Environment*, vol. 1, no. 3, pp. 337–346, 2012. [Online]. Available: https://onlinelibrary.wiley.com/doi/abs/10.1002/wene.43

[29] Y. D. Ko, Y. J. Jang, and S. Jeong, "Mathematical modeling and optimization of

the automated wireless charging electric transportation system," in *IEEE International Conference on Automation Science and Engineering*, 2012, pp. 250–255.

[30] B. Regensburger, A. Kumar, S. Sinha, and K. Afridi, "High-performance 13.56-mhz large air-gap capacitive wireless power transfer system for electric vehicle charging," in *IEEE Workshop on Control and Modeling for Power Electronics*, 2018, pp. 1–4.

[31] S. K. Samal, D. P. Kar, P. K. Sahoo, S. Bhuyan, and S. N. Das, "Analysis of the effect of design parameters on the power transfer efficiency of resonant inductive coupling based wireless ev charging system," in *Innovations in Power and Advanced Computing Technologies*, 2017, pp. 1–4.

[32] I.-G. Sîrbu and L. Mandache, "Comparative analysis of different topologies for wireless power transfer systems," in *IEEE International Conference on Environment and Electrical Engineering and IEEE Industrial and Commercial Power Systems Europe*, 2017, pp. 1–6.

[33] A. A. S. Mohamed, A. Berzoy, and O. A. Mohammed, "Physics-based fe model and analytical verification of bi-directional inductive wireless power transfer system," in *IEEE/ACES International Conference on Wireless Information Technology and Systems and Applied Computational Electromagnetics*, 2016, pp. 1–2.

[34] G. Liu and B. Zhang, "Dual-coupled robust wireless power transfer based on

parity-time-symmetric model," *Chinese Journal of Electrical Engineering*, vol. 4, no. 2, pp. 50–55, 2018.

[35] D. Vincent, S. Chakraborty, P. S. Huynh, and S. S. Williamson, "Efficiency analysis of a 7.7 kw inductive wireless power transfer system with parallel displacement," in *IEEE International Conference on Industrial Electronics for Sustainable Energy Systems*, 2018, pp. 409–414.

[36] Z. Zhang, K. T. Chau, C. Liu, F. Li, and T. W. Ching, "Quantitative analysis of mutual inductance for optimal wireless power transfer via magnetic resonant coupling," *IEEE Transactions on Magnetics*, vol. 50, no. 11, pp. 1–4, 2014.

[37] A. Sharma and D. Kathuria, "Performance analysis of a wireless power transfer system based on inductive coupling," in *International Conference on Computing, Power and Communication Technologies*, 2018, pp. 55–59.

[38] C. R. Sullivan and R. Y. Zhang, "Simplified design method for litz wire," in *IEEE Applied Power Electronics Conference and Exposition*, 2014, pp. 2667–2674.

[39] B. Kallel, O. Kanoun, T. Keutel, and C. Viehweger, "Improvement of the efficiency of miso configuration in inductive power transmission in case of coils misalignment," in *IEEE International Instrumentation and Measurement Technology Conference Proceedings*, 2014, pp. 856–861.

[40] A. A. Mohamed, D. Allen, T. Youssef, and O. Mohammed, "Optimal design of

high frequency h-bridge inverter for wireless power transfer systems in ev applications," in *International Conference on Environment and Electrical Engineering*. IEEE, 2016, pp. 1–6.

[41] Y. Yang, J. Cui, and X. Cui, "Design and analysis of magnetic coils for optimizing the coupling coefficient in an electric vehicle wireless power transfer system," *Energies*, vol. 13, no. 16, p. 4143, 2020.

[42] A. A. Mohamed, A. Berzoy, F. G. de Almeida, and O. Mohammed, "Steady-state performance assessment of different compensation topologies in two-way iwpt system for ev ancillary services," in *IEEE Industry Applications Society Annual Meeting*. IEEE, 2016, pp. 1–8.

[43] A. A. Mohamed, A. Berzoy, F. de Almeida, and O. Mohammed, "Modeling and assessment analysis of various compensation topologies in bidirectional iwpt system for ev applications," *IEEE Transactions on Industry Applications*, vol. 53, no. 5, pp. 4973–4984, 2017.

[44] M. Banzi and M. Shiloh, *Getting started with Arduino*. Maker Media, Inc., 2022.

[45] S.-E. Oltean, "Mobile robot platform with arduino uno and raspberry pi for autonomous navigation," *Procedia Manufacturing*, vol. 32, pp. 572–577, 2019.

[46] Y. A. Badamasi, "The working principle of an arduino," in *International Conference on Electronics, Computer and Computation*, 2014, pp. 1–4.

[47] S. Ranjit and M. Abbod, "Research and integration of iot based solar photovoltaic panel health monitoring system," *Scientific Research Publishing: Advances in Internet of Things*, 2018.

[48] M. Tastan, "Real time remote monitoring and control application with new generation iot controller for smart home applications," *Süleyman Demirel Üniversitesi Fen Bilimleri Enstitüsü dergisi*, vol. 23, no. 2, pp. 481–487, 2019.

[49] L. Syafa'ah, A. E. Minarno, F. D. S. Sumadi, and D. A. P. Rahayu, "Esp 8266 for control and monitoring in smart home application," in *International Conference on Computer Science, Information Technology, and Electrical Engineering*, 2019, pp. 123–128.

[50] Muliadi, M. Y. Fahrezi, I. S. Areni, E. Palantel, and A. Achmad, "A smart home energy consumption monitoring system integrated with internet connection," in *IEEE International Conference on Communication, Networks and Satellite (Comnetsat)*, 2020, pp. 75–80.

[51] O. Akintade, T. Yesufu, and L. Kehinde, "Development of power consumption models for esp8266-enabled low-cost iot monitoring nodes," *Advances in Internet of Things*, vol. 09, pp. 1–14, 01 2019.

[52] C.-C. Hua, H.-R. Chen, and Y.-H. Fang, "Inductive power transmission technology for li-ion battery charger," in *IEEE International Conference on Power Electronics and Drive Systems*, 2013, pp. 788–792.

[53] J. Benesty, J. Chen, Y. Huang, and I. Cohen, "Pearson correlation coefficient," in *Noise reduction in speech processing*. Springer, 2009, pp. 1–4.

[54] The Mathworks, "Correlation Coefficients r," 2019, (Accessed 16 October 2019). [Online]. Available: https://www.mathworks.com/help/matlab/ref/corrcoef.html

[55] The Mathworks , "Quantile-Quantile Plot r," 2019, (Accessed 16 October 2019). [Online]. Available: https://www.mathworks.com/help/stats/qqplot.html

[56] M. Eghtesadi, "Inductive power transfer to an electric vehicle-analytical model," in *IEEE Conference on Vehicular Technology*, May 1990, pp. 100–104.

[57] Weaver, Wayne W., Nina Mahmoudian, and G. Parker, "Autonomous mobile power blocks for prepositioned power conversion and distribution," in *TARDEC Ground Vehicle Systems Engineering and Technology Symposium*, 2012.

Appendix A

Control Code

A.1 microgrid_ws bus_agent_CSG.py

```
Python 3.6.4 (v3.6.4:d48eceb, Dec 19 2017, 06:04:45) [↩
   MSC v.1900 32 bit (Intel)] on win32
Type "copyright", "credits" or "license()" for more ↩
   information.
>>>
    #<!-- rosserial for primary coil on arduino -->
    <node pkg="rosserial_python" type="serial_node.py" ↩
       name="nearfieldComms">
    <param name="port" value="/dev/ttyACM0"/>
    </node>
```

```
    <!-- rosserial for load communication with esp8266's↩
        -->
    <node pkg="rosserial_server" type="socket_node" name↩
       ="loadComms">
    </node>


#Logging for ROS topics:

    #!/usr/bin/env python

    import xlsxwriter
    from datetime import datetime
    import rospy
    import tf2_ros
    from sensor_msgs.msg import NavSatFix
    from nav_msgs.msg import Odometry
    from std_msgs.msg import Float32, String
    from geometry_msgs.msg import ↩
       PoseWithCovarianceStamped
    from math import isnan
    import numpy as np
    from tf import transformations as tfs
    from diagnostic_msgs.msg import DiagnosticArray


    class mcvwb():

        def __init__(self):
            wbname = "/home/administrator/huskycostlogs↩
               /" + str(datetime.now()) + ".xlsx"
            print wbname
            try:
```

```
        self.workbook = xlsxwriter.Workbook(↩
            wbname)
        self.worksheet = self.workbook.↩
            add_worksheet()
    except Exception as e:
        print(repr(e))
    self.row=0
    self.timecol=0
    self.ekfcolx = 1
    self.ekfcoly = 2
    self.ekfcoltheta = 3
    self.nfcolA = 4
    self.nfcolV = 5
    self.nfcolW = 6

    self.x = None
    self.y = None
    self.theta = None
    self.A = None
    self.V = None

    try:
        self.worksheet.write(self.row,self.↩
            timecol,"time")
        self.worksheet.write(self.row,self.↩
            ekfcolx,"ekf x")
        self.worksheet.write(self.row,self.↩
            ekfcoly,"ekf y")
        self.worksheet.write(self.row,self.↩
            ekfcoltheta,"ekf theta")
        self.worksheet.write(self.row,self.↩
            nfcolA,"amps")
        self.worksheet.write(self.row,self.↩
            nfcolV,"volts")
```

```
            except Exception as e:
                print(repr(e))
            self.row += 1

            def ekfback(data):
                self.x=data.pose.pose.position.x
                self.y=data.pose.pose.position.y
                self.theta = tfs.euler_from_quaternion([↩
                   data.pose.pose.orientation.x,data.pose↩
                   .pose.orientation.y,
                    data.pose.pose.orientation.z,data.↩
                       pose.pose.orientation.w],axes='↩
                       sxyz')[2]

 def nfVback(data):
 if "husky_node: system_status" in data.status:
                print(data.status)
# for row in enumerate(data.status.values):
# if row.status.values.key=="Battery Voltage":
# self.V=float(row.status.values.value)
            try:
                self.worksheet.write(self.row,self.↩
                   timecol,rospy.get_time())

                self.worksheet.write(self.row,self.↩
                   ekfcolx,self.x)
                self.worksheet.write(self.row,self.↩
                   ekfcoly,self.y)
                self.worksheet.write(self.row,self.↩
                   ekfcoltheta,self.theta)

                self.worksheet.write(self.row,self.↩
                   nfcolA,self.A)
```

```
                    self.worksheet.write(self.row,self.↩
                        nfcolV,self.V)
                    self.worksheet.write(self.row,self.↩
                        nfcolW,np.multiply(self.A,self.V))

                except Exception as e:
                    print(repr(e))
                self.row += 1

            def nfAback(data):
                self.A=data.data

            rospy.Subscriber('odometry/filtered',↩
                Odometry,ekfback)
            rospy.Subscriber('batteryCurrent',Float32,↩
                nfAback)
            rospy.Subscriber('diagnostics',↩
                DiagnosticArray,nfVback)


if __name__=='__main__':
    try:
        rospy.init_node('logGPStoCSV',↩
            disable_signals=True)
        bob = mcvwb()
        rospy.spin()
    except Exception as e:
        print(repr(e))
    finally:
        bob.workbook.close()
        print "DONE!!!"
```

A.2 V_C_log_ROS_ina219.ino

```
#include <ros.h>
#include <std_msgs/Float32.h>
#include <Wire.h>
#include <Adafruit_INA219.h>

Adafruit_INA219 ina219;

ros::NodeHandle  nh;

std_msgs::Float32 amps_msg;
std_msgs::Float32 volts_msg;
std_msgs::Float32 power_msg;
ros::Publisher wirelessAmps("wirelessAmps", &amps_msg);
ros::Publisher wirelessVolts("wirelessVolts", &volts_msg↩
  );
ros::Publisher wirelessPower("wirelessPower", &power_msg↩
  );

//int offset =0;// set offset value
//#define acs712 A0
//#define MHV A1
//float vpp = 0.0048828125;
//float sensitivity = 0.100;

void setup() {
  nh.initNode();
  nh.advertise(wirelessAmps);
  nh.advertise(wirelessVolts);
  nh.advertise(wirelessPower);
```

```
  uint32_t currentFrequency;
  // Initialize the INA219.
  // By default the initialization will use the largest range (32V, 2A).  However
  // you can call a setCalibration function to change this range (see comments).
  ina219.begin();
  // To use a slightly lower 32V, 1A range (higher precision on amps):
  //ina219.setCalibration_32V_1A();
  // Or to use a lower 16V, 400mA range (higher precision on volts and amps):
  //ina219.setCalibration_16V_400mA();

}

long publisher_timer;

void loop()
{
  if (millis() > publisher_timer)
  {
    // voltage and current sensor
    //int volt = analogRead(MHV);// read the input
    //double voltage = map(volt,0,1023, 0, 2500) + offset;// map 0-1023 to 0-2500 and add correction offset

    //voltage /=100;// divide by 100 to get the decimal values

    //int counts = analogRead(acs712);
    //float volts = counts * vpp;
```

```
    //volts -= 2.5;

    //float amperage = volts / sensitivity;

    //float power = voltage*amperage;

  float shuntvoltage = ina219.getShuntVoltage_mV();
  float busvoltage = ina219.getBusVoltage_V();


    amps_msg.data = ina219.getCurrent_mA();
    volts_msg.data = busvoltage + (shuntvoltage / 1000);
    power_msg.data = ina219.getPower_mW();

    wirelessAmps.publish(&amps_msg);
    wirelessVolts.publish(&volts_msg);
    wirelessPower.publish(&power_msg);

    publisher_timer = millis() + 999; //publish once a ↩
       second
  }

  nh.spinOnce();

  delay(1);
}
```

A.3 V_C_log_RTCwSD_ina219.ino

```
#include "SD.h"
```

```
#include <Wire.h>
#include "RTClib.h"
#include <Adafruit_INA219.h>

Adafruit_INA219 ina219;

#define LOG_INTERNAL 1000
#define ECHO_TO_SERIAL 1
#define WAIT_TO_START 0

//int offset =0;// set offset value
//#define acs712 A0
//#define MHV A1
//float vpp = 0.0048828125;
//float sensitivity = 0.100;

RTC_PCF8523 rtc;

const int chipSelect = 10;

File logfile;
String filename;

void setup() {
  Serial.begin(115200);// initialize serial monitor

  if (! rtc.begin()) {
    Serial.println("Couldn't find RTC");
    while (1);
  }

  if (! rtc.initialized()) {
    Serial.println("RTC is NOT running!");
```

```
  // following line sets the RTC to the date & time ↩
     this sketch was compiled
   rtc.adjust(DateTime(F(__DATE__), F(__TIME__)));
  // This line sets the RTC with an explicit date & ↩
     time, for example to set
  // January 21, 2014 at 3am you would call:
  // rtc.adjust(DateTime(2014, 1, 21, 3, 0, 0));
}

Serial.print("Initializing SD card....");
pinMode(10, OUTPUT);

if(!SD.begin(chipSelect))
{
  Serial.println("Card failed or card not present");
  return;
}
Serial.println("Card initialized.");

DateTime now = rtc.now();
filename = String(now.day())+String(now.hour())+String↩
   (now.minute())+String(now.second())+".csv";
Serial.println(filename);

logfile = SD.open(filename.c_str(), FILE_WRITE);
if (logfile){
  Serial.println("time, amps, volts, watts");
  logfile.println("time,amps,volts,watts");
  logfile.close();
}
else {
  // if the file didn't open, print an error:
  Serial.println("error opening "+filename);
}
```

```
    uint32_t currentFrequency;
  // Initialize the INA219.
  // By default the initialization will use the largest ↩
     range (32V, 2A).  However
  // you can call a setCalibration function to change ↩
     this range (see comments).
  ina219.begin();
  // To use a slightly lower 32V, 1A range (higher ↩
     precision on amps):
  //ina219.setCalibration_32V_1A();
  // Or to use a lower 16V, 400mA range (higher ↩
     precision on volts and amps):
  //ina219.setCalibration_16V_400mA();
}

void loop()
{
    DateTime now = rtc.now();

  // voltage and current sensor
//  int volt = analogRead(MHV);// read the input
//  double voltage = map(volt,0,1023, 0, 2500) + offset↩
   ;// map 0-1023 to 0-2500 and add correction offset

//  voltage /=100;// divide by 100 to get the decimal ↩
   values

  //int counts = analogRead(acs712);
  //float volts = counts * vpp;
  //volts -= 2.5;

  //float amperage = volts / sensitivity;
```

```
//  float power = voltage*amperage;

  float voltage = ina219.getBusVoltage_V();
  float amperage = ina219.getCurrent_mA();
  float power = ina219.getPower_mW();
    float shuntvoltage = ina219.getShuntVoltage_mV();

  float loadvoltage = voltage + (shuntvoltage / 1000);

  logfile = SD.open(filename.c_str(), FILE_WRITE);
  if (logfile){
    logfile.print(now.unixtime());
    logfile.print(",");
    logfile.print(amperage);
    logfile.print(",");
    logfile.print(loadvoltage);
    logfile.print(",");
    logfile.print(power);
    logfile.println();
    logfile.close();
  }
  else {
    // if the file didn't open, print an error:
    Serial.println("error opening "+filename);
  }

  Serial.print(now.unixtime());
  Serial.print(",");
  Serial.print(amperage);
  Serial.print(",");
  Serial.print(voltage);
  Serial.print(",");
  Serial.println(power);
```

```
  delay(1000);
}
```

A.4 V_C_log_ROS_Esp32.ino

```
/*
 * rosserial Publisher Example
 * Prints "hello world!"
 * This intend to connect to a Wifi Access Point
 * and a rosserial socket server.
 * You can launch the rosserial socket server with
 * roslaunch rosserial_server socket.launch
 * The default port is 11411
 *
 */



//to modify this script depending on which esp is ↩
   running it, change the numbers in the ros
//topic name definitions and change the static IP that ↩
   the esp is assigned




//#include <ESP8266WiFi.h>
#include <WiFi.h>
#include <ros.h>
//#include <std_msgs/String.h>
```

```
#include <std_msgs/Float32.h>
#include <Wire.h>
#include <Adafruit_INA219.h>

const char* ssid     = "microgrid";
const char* password = "microgrid";

//const char* ssid     = "hug2g796989";
//const char* password = "priest92nail";

// Set the rosserial socket server IP address
IPAddress server(192,168,1,11);

//IPAddress server(192,168,42,3);

// Set the rosserial socket server port
const uint16_t serverPort = 11411;

std_msgs::Float32 amps_msg;
std_msgs::Float32 volts_msg;
std_msgs::Float32 power_msg;
ros::Publisher wirelessAmps("wirelessAmps3", &amps_msg);
ros::Publisher wirelessVolts("wirelessVolts3", &↩
   volts_msg);
ros::Publisher wirelessPower("wirelessPower3", &↩
   power_msg);
ros::Publisher loadAmps("loadAmps3", &amps_msg);
ros::Publisher loadVolts("loadVolts3", &volts_msg);
ros::Publisher loadPower("loadPower3", &power_msg);

Adafruit_INA219 ina219;
Adafruit_INA219 loadina219(0x41);

ros::NodeHandle nh;
```

```
// Make a chatter publisher
//std_msgs::String str_msg;
//ros::Publisher chatter("chatter1", &str_msg);

// Be polite and say hello
//char hello[13] = "Load 2!";

void setup()
{
  // Use ESP8266 serial to monitor the process
  Serial.begin(115200);
  Serial.println();
  Serial.print("Connecting to ");
  Serial.println(ssid);

  // Connect the ESP8266 the the wifi AP
  WiFi.begin(ssid, password);
  IPAddress ip(192,168,0,37); //#1 .35, #2 .36, #3 .37
IPAddress gateway(192,168,0,1);
IPAddress subnet(255,255,0,0);

//  IPAddress ip(192,168,42,36);
//IPAddress gateway(192,168,42,1);

WiFi.config(ip, gateway, subnet);
  while (WiFi.status() != WL_CONNECTED) {
    delay(500);
    Serial.print(".");
  }
  Serial.println("");
  Serial.println("WiFi connected");
  Serial.println("IP address: ");
  Serial.println(WiFi.localIP());
```

```
// Set the connection to rosserial socket server
nh.getHardware()->setConnection(server, serverPort);
nh.initNode();

// Another way to get IP
Serial.print("IP = ");
Serial.println(nh.getHardware()->getLocalIP());

// Start to be polite
//nh.advertise(chatter);


nh.advertise(wirelessAmps);
nh.advertise(wirelessVolts);
nh.advertise(wirelessPower);
nh.advertise(loadAmps);
nh.advertise(loadVolts);
nh.advertise(loadPower);

uint32_t currentFrequency;
// Initialize the INA219.
// By default the initialization will use the largest ↩
   range (32V, 2A).  However
// you can call a setCalibration function to change ↩
   this range (see comments).
ina219.begin();
// To use a slightly lower 32V, 1A range (higher ↩
   precision on amps):
//ina219.setCalibration_32V_1A();
// Or to use a lower 16V, 400mA range (higher ↩
   precision on volts and amps):
//ina219.setCalibration_16V_400mA();
loadina219.begin();
```

```
}

long publisher_timer;

void loop()
{
  if (millis() > publisher_timer)
  {
    publisher_timer = millis() + 99;


  if (nh.connected()) {
    Serial.println("Connected");
    // Say hello
    //str_msg.data = hello;
    //chatter.publish( &str_msg );
  } else {
    Serial.println("Not Connected");
  }

//get data from the secondary module and publish to ROS
    float shuntvoltage = ina219.getShuntVoltage_mV();
    float busvoltage = ina219.getBusVoltage_V();

    amps_msg.data = ina219.getCurrent_mA();
    volts_msg.data = busvoltage + (shuntvoltage / 1000);
    power_msg.data = ina219.getPower_mW();

    wirelessAmps.publish(&amps_msg);
    wirelessVolts.publish(&volts_msg);
    wirelessPower.publish(&power_msg);

//get data from the load and publish to ROS
```

```
    float loadshuntvoltage = loadina219.↩
       getShuntVoltage_mV();
    float loadbusvoltage = loadina219.getBusVoltage_V();

    amps_msg.data = loadina219.getCurrent_mA();
    volts_msg.data = busvoltage + (shuntvoltage / 1000);
    power_msg.data = loadina219.getPower_mW();

    loadAmps.publish(&amps_msg);
    loadVolts.publish(&volts_msg);
    loadPower.publish(&power_msg);

  }

  nh.spinOnce();

  delay(1);
}
```

A.5 V_C_log_ROS_Esp8266.ino

```
/*
 * rosserial Publisher Example
 * Prints "hello world!"
 * This intend to connect to a Wifi Access Point
 * and a rosserial socket server.
 * You can launch the rosserial socket server with
 * roslaunch rosserial_server socket.launch
 * The default port is 11411
 *
```

```
 */


//to modify this script depending on which esp is running it, change the numbers in the ros
//topic name definitions and change the static IP that the esp is assigned




#include <ESP8266WiFi.h>
//#include <WiFi.h>
#include <ros.h>
//#include <std_msgs/String.h>
#include <std_msgs/Float32.h>
#include <Wire.h>
#include <Adafruit_INA219.h>

const char* ssid     = "microgrid";
const char* password = "microgrid";

//const char* ssid     = "hug2g796989";
//const char* password = "priest92nail";

// Set the rosserial socket server IP address
IPAddress server(192,168,1,11);

//IPAddress server(192,168,42,3);

// Set the rosserial socket server port
const uint16_t serverPort = 11411;
```

```
std_msgs::Float32 amps_msg;
std_msgs::Float32 volts_msg;
std_msgs::Float32 power_msg;
ros::Publisher wirelessAmps("wirelessAmps1", &amps_msg);
ros::Publisher wirelessVolts("wirelessVolts1", &↩
   volts_msg);
ros::Publisher wirelessPower("wirelessPower1", &↩
   power_msg);
//ros::Publisher loadAmps("loadAmps2", &amps_msg);
//ros::Publisher loadVolts("loadVolts2", &volts_msg);
//ros::Publisher loadPower("loadPower2", &power_msg);

Adafruit_INA219 ina219;
//Adafruit_INA219 loadina219(0x41);

ros::NodeHandle nh;

// Make a chatter publisher
//std_msgs::String str_msg;
//ros::Publisher chatter("chatter1", &str_msg);

// Be polite and say hello
//char hello[13] = "Load 2!";

void setup()
{
  // Use ESP8266 serial to monitor the process
  Serial.begin(115200);
  Serial.println();
  Serial.print("Connecting to ");
  Serial.println(ssid);

  // Connect the ESP8266 the the wifi AP
  WiFi.begin(ssid, password);
```

```
  IPAddress ip(192,168,0,35); //#1 .35, #2 .36, #3 .37
IPAddress gateway(192,168,0,1);
IPAddress subnet(255,255,0,0);

//  IPAddress ip(192,168,42,36);
//IPAddress gateway(192,168,42,1);

WiFi.config(ip, gateway, subnet);
  while (WiFi.status() != WL_CONNECTED) {
    delay(500);
    Serial.print(".");
  }
  Serial.println("");
  Serial.println("WiFi connected");
  Serial.println("IP address: ");
  Serial.println(WiFi.localIP());

  // Set the connection to rosserial socket server
  nh.getHardware()->setConnection(server, serverPort);
  nh.initNode();

  // Another way to get IP
  Serial.print("IP = ");
  Serial.println(nh.getHardware()->getLocalIP());

  // Start to be polite
  //nh.advertise(chatter);


  nh.advertise(wirelessAmps);
  nh.advertise(wirelessVolts);
  nh.advertise(wirelessPower);
//  nh.advertise(loadAmps);
//  nh.advertise(loadVolts);
```

```
//  nh.advertise(loadPower);

  uint32_t currentFrequency;
  // Initialize the INA219.
  // By default the initialization will use the largest ↩
     range (32V, 2A).  However
  // you can call a setCalibration function to change ↩
     this range (see comments).
  ina219.begin();
  // To use a slightly lower 32V, 1A range (higher ↩
     precision on amps):
  //ina219.setCalibration_32V_1A();
  // Or to use a lower 16V, 400mA range (higher ↩
     precision on volts and amps):
  //ina219.setCalibration_16V_400mA();
//  loadina219.begin();
}

long publisher_timer;

void loop()
{
  if (millis() > publisher_timer)
  {
    publisher_timer = millis() + 99;


  if (nh.connected()) {
    Serial.println("Connected");
    // Say hello
    //str_msg.data = hello;
    //chatter.publish( &str_msg );
  } else {
    Serial.println("Not Connected");
```

```
  }

//get data from the secondary module and publish to ROS
    float shuntvoltage = ina219.getShuntVoltage_mV();
    float busvoltage = ina219.getBusVoltage_V();

    amps_msg.data = ina219.getCurrent_mA();
    volts_msg.data = busvoltage + (shuntvoltage / 1000);
    power_msg.data = ina219.getPower_mW();

    wirelessAmps.publish(&amps_msg);
    wirelessVolts.publish(&volts_msg);
    wirelessPower.publish(&power_msg);

//get data from the load and publish to ROS
/*    float loadshuntvoltage = loadina219.↩
   getShuntVoltage_mV();
    float loadbusvoltage = loadina219.getBusVoltage_V();

    amps_msg.data = loadina219.getCurrent_mA();
    volts_msg.data = loadbusvoltage + (loadshuntvoltage ↩
       / 1000);
    power_msg.data = loadina219.getPower_mW();

    loadAmps.publish(&amps_msg);
    loadVolts.publish(&volts_msg);
    loadPower.publish(&power_msg);
*/
  }

  nh.spinOnce();

  delay(1);
}
```

Appendix B

Copyright Permissions

The copyright permissions and correspondences for the papers used in this thesis are provided in this section.

Michigan Tech

Carl Greene <carlg@mtu.edu>

Request for Permission to Publish Content

2 messages

Carl Greene <carlg@mtu.edu> Wed, Mar 10, 2021 at 9:24 AM
To: Casey Majhor <cmajhor@mtu.edu>

Mr. Majhor,

I am requesting permission to reuse content from the recent publication:

Recharging of Distributed Loads via Schedule Optimization with Autonomous Mobile Energy Assets, IEEE 2020 Aerospace Conference
https://ieeexplore.ieee.org/document/9172729

As the lead author of this work, I would like you to be aware that portions of this paper would be used in drafting my master's thesis at Michigan Technological University.

Let me know at your earliest convenience.

Regards,
Carl Greene

Casey Majhor <cmajhor@mtu.edu> Wed, Mar 10, 2021 at 9:31 AM
To: Carl Greene <carlg@mtu.edu>

Hi Carl,

You have my permission to reuse it for your thesis.

-Casey Majhor
[Quoted text hidden]

Michigan Tech

Carl Greene <carlg@mtu.edu>

Permission to use content

2 messages

Carl Greene <carlg@mtu.edu> Wed, Mar 10, 2021 at 9:28 AM
To: John Naglak <jenaglak@mtu.edu>

Mr. Naglak,

I am requesting permission to reuse content from the recent publication:

Autonomous Power Grid Formation for Surface Assets Using Multiple Unmanned Ground Vehicles, IEEE 2020 Aerospace Conference
https://ieeexplore.ieee.org/document/9172615

As the lead author of this work, I would like you to be aware that portions of this paper would be used in drafting my master's thesis at Michigan Technological University.

Let me know at your earliest convenience.

Regards,
Carl Greene

John Naglak <jenaglak@mtu.edu> Wed, Mar 10, 2021 at 3:55 PM
To: Carl Greene <carlg@mtu.edu>

Yes, I approve.

John Naglak
[Quoted text hidden]

Recharging of Distributed Loads via Schedule Optimization with Autonomous Mobile Energy Assets

Conference Proceedings: 2020 IEEE Aerospace Conference

Author: Casey D. Majhor; John E. Naglak; Carl S. Greene; Wayne W. Weaver; Jeremy P. Bos

Publisher: IEEE

Date: 7-14 March 2020

Thesis / Dissertation Reuse

The IEEE does not require individuals working on a thesis to obtain a formal reuse license, however, you may print out this statement to be used as a permission grant:

Requirements to be followed when using any portion (e.g., figure, graph, table, or textual material) of an IEEE copyrighted paper in a thesis:

1) In the case of textual material (e.g., using short quotes or referring to the work within these papers) users must give full credit to the original source (author, paper, publication) followed by the IEEE copyright line © 2011 IEEE.
2) In the case of illustrations or tabular material, we require that the copyright line © [Year of original publication] IEEE appear prominently with each reprinted figure and/or table.
3) If a substantial portion of the original paper is to be used, and if you are not the senior author, also obtain the senior author's approval.

Requirements to be followed when using an entire IEEE copyrighted paper in a thesis:

1) The following IEEE copyright/ credit notice should be placed prominently in the references: © [year of original publication] IEEE. Reprinted, with permission, from [author names, paper title, IEEE publication title, and month/year of publication]
2) Only the accepted version of an IEEE copyrighted paper can be used when posting the paper or your thesis on-line.
3) In placing the thesis on the author's university website, please display the following message in a prominent place on the website: In reference to IEEE copyrighted material which is used with permission in this thesis, the IEEE does not endorse any of [university/educational entity's name goes here]'s products or services. Internal or personal use of this material is permitted. If interested in reprinting/republishing IEEE copyrighted material for advertising or promotional purposes or for creating new collective works for resale or redistribution, please go to http://www.ieee.org/publications_standards/publications/rights/rights_link.html to learn how to obtain a License from RightsLink.

If applicable, University Microfilms and/or ProQuest Library, or the Archives of Canada may supply single copies of the dissertation.

BACK CLOSE WINDOW

Autonomous Power Grid Formation for Surface Assets Using Multiple Unmanned Ground Vehicles

Conference Proceedings: 2020 IEEE Aerospace Conference

Author: John Naglak

Publisher: IEEE

Date: March 2020

Thesis / Dissertation Reuse

The IEEE does not require individuals working on a thesis to obtain a formal reuse license, however, you may print out this statement to be used as a permission grant:

Requirements to be followed when using any portion (e.g., figure, graph, table, or textual material) of an IEEE copyrighted paper in a thesis:

1) In the case of textual material (e.g., using short quotes or referring to the work within these papers) users must give full credit to the original source (author, paper, publication) followed by the IEEE copyright line © 2011 IEEE.
2) In the case of illustrations or tabular material, we require that the copyright line © [Year of original publication] IEEE appear prominently with each reprinted figure and/or table.
3) If a substantial portion of the original paper is to be used, and if you are not the senior author, also obtain the senior author's approval.

Requirements to be followed when using an entire IEEE copyrighted paper in a thesis:

1) The following IEEE copyright/ credit notice should be placed prominently in the references: © [year of original publication] IEEE. Reprinted, with permission, from [author names, paper title, IEEE publication title, and month/year of publication]
2) Only the accepted version of an IEEE copyrighted paper can be used when posting the paper or your thesis on-line.
3) In placing the thesis on the author's university website, please display the following message in a prominent place on the website: In reference to IEEE copyrighted material which is used with permission in this thesis, the IEEE does not endorse any of [university/educational entity's name goes here]'s products or services. Internal or personal use of this material is permitted. If interested in reprinting/republishing IEEE copyrighted material for advertising or promotional purposes or for creating new collective works for resale or redistribution, please go to http://www.ieee.org/publications_standards/publications/rights/rights_link.html to learn how to obtain a License from RightsLink.

If applicable, University Microfilms and/or ProQuest Library, or the Archives of Canada may supply single copies of the dissertation.

BACK CLOSE WINDOW

IEEE Requesting permission to reuse content from an IEEE publication

Near Field Wireless Power Transfer via Robotic Feedback Control

Conference Proceedings: 2020 IEEE Aerospace Conference
Author: Carl Greene
Publisher: IEEE
Date: March 2020

Thesis / Dissertation Reuse

The IEEE does not require individuals working on a thesis to obtain a formal reuse license, however, you may print out this statement to be used as a permission grant:

Requirements to be followed when using any portion (e.g., figure, graph, table, or textual material) of an IEEE copyrighted paper in a thesis:

1) In the case of textual material (e.g., using short quotes or referring to the work within these papers) users must give full credit to the original source (author, paper, publication) followed by the IEEE copyright line © 2011 IEEE.
2) In the case of illustrations or tabular material, we require that the copyright line © [Year of original publication] IEEE appear prominently with each reprinted figure and/or table.
3) If a substantial portion of the original paper is to be used, and if you are not the senior author, also obtain the senior author's approval.

Requirements to be followed when using an entire IEEE copyrighted paper in a thesis:

1) The following IEEE copyright/ credit notice should be placed prominently in the references: © [year of original publication] IEEE. Reprinted, with permission, from [author names, paper title, IEEE publication title, and month/year of publication]
2) Only the accepted version of an IEEE copyrighted paper can be used when posting the paper or your thesis on-line.
3) In placing the thesis on the author's university website, please display the following message in a prominent place on the website: In reference to IEEE copyrighted material which is used with permission in this thesis, the IEEE does not endorse any of [university/educational entity's name goes here]'s products or services. Internal or personal use of this material is permitted. If interested in reprinting/republishing IEEE copyrighted material for advertising or promotional purposes or for creating new collective works for resale or redistribution, please go to http://www.ieee.org/publications_standards/publications/rights/rights_link.html to learn how to obtain a License from RightsLink.

If applicable, University Microfilms and/or ProQuest Library, or the Archives of Canada may supply single copies of the dissertation.

BACK CLOSE WINDOW